HIGH RESOLUTION IMAGING OF EARLY, SUBCLINICAL CARTILAGE INJURIES: IMPLICATIONS FOR THE DIAGNOSIS AND TREATMENT OF POST-TRAUMATIC OSTEOARTHRITIS

A Dissertation

Presented to the Faculty of the Graduate School

of Cornell University

In Partial Fulfillment of the Requirements for the Degree of

Doctor of Philosophy

by

Kira Diane Novakofski

January 2014

HIGH RESOLUTION IMAGING OF EARLY, SUBCLINICAL CARTILAGE INJURIES: IMPLICATIONS FOR THE DIAGNOSIS AND TREATMENT OF POST-TRAUMATIC OSTEOARTHRITIS

Kira Diane Novakofski, Ph.D.

Cornell University 2014

Osteoarthritis (OA) is a degenerative disease. Currently, there are no treatments to restore damaged cartilage to its native state. Joint injury increases the risk of developing post-traumatic OA (PTOA). Subtle cartilage injury that may progress to PTOA cannot be detected with current clinical imaging modalities. If subtle cartilage injury is detectable, PTOA can be better understood to develop treatments targeting early disease progression. The goal of this dissertation was to evaluate methods for detecting, characterizing, and treating early cartilage injury.

Multiphoton microscopy (MPM) can provide high resolution details of live, intact tissue. The purpose of the first study was to validate the use of MPM to detect subtle cartilage damage. The results confirmed the ability of MPM to resolve structural changes and cell death in cartilage immediately after injury. This suggests future application of MPM in the clinic for early diagnosis or in the laboratory to perform longitudinal studies not currently possible due to the necessity of histological processing.

In the second study, cartilage and its resiliency to injury were evaluated among eight major joints to determine if there are different susceptibilities to injury in different joints. The structure of articular cartilage and prevalence of OA vary among joints, but typically results from work performed within a single joint are applied to other joints. The results from the second study showed that some joints have more

cellular death and/or decrease anabolic gene expression than other joints after receiving the same injury, which suggests the need for joint specific treatments.

The third study examined the role of oxygen in the development of PTOA. Cartilage is avascular and has limited oxygen supply. Oxygen tension may be increased in arthritic joints, yet short exposure to high oxygen tension is beneficial to uninjured cartilage. In this final study, the effect of increased oxygen tension on cartilage viability after injury was evaluated. The immediate application of hyperoxic treatment minimized cell death after injury, suggesting that the immediate application of high oxygen following injury may be chondroprotective. These findings have implications in future treatments that could minimize the effect of cartilage injury and development of PTOA.

BIOGRAPHICAL SKETCH

Kira Diane Novakofski was born in Wamego, Kansas on September 20th, 1983 to Todd Novakofski and Pat Zbikowski. She grew up in Ladysmith, Wisconsin and graduated from Ladysmith High School in May 2001 as valedictorian. She then attended the University of Wisconsin-Madison, where she completed her B.S. in May 2004 in biochemistry. Ms. Novakofski moved to Ithaca, NY in August 2004 to begin graduate work in the Field of Comparative Biomedical Sciences at Cornell University. Having a long term interest in osteoarthritis from her experience with horses, Ms. Novakofski began to work with Dr. Lisa Fortier in January 2005 to focus on studying the mechanism of osteoarthritis pathogenesis. She completed her M.S. in January 2007, with her M.S. thesis written on chondrocyte signaling.

Ms. Novakofski continued to pursue orthopedic-focused research in Dr. Fortier's laboratory and was admitted to the Ph.D. program in the Graduate Field of Comparative Biomedical Sciences in August 2010. Ms. Novakofski's applied for and was awarded a competitive fellowship through the Clinical and Translational Science Center of Weill Cornell Medical College. During her Ph.D. work, Ms. Novakofski continued to develop her interest in osteoarthritis and cartilage research, with an emphasis on bench-to-bedside research. Combined with her interest in athletic performance, she plans to continue work in clinical translational research in the orthopedic field with the goal of becoming more directly involved in the medical field.

Dedicated to those who have inspired and encouraged my journey.

ACKNOWLEDGMENTS

I have been fortunate to have wonderful family and friends who have supported me during my Ph.D. It has been a long road to get to this point, and I would not have done it without being surrounded by such amazing people.

First and foremost, I want to thank my parents, Todd Novakofski and Pat Zbikowski, for their continued support. They have always encouraged me to follow my dreams and pursue my goals. I would not be where I am today without them, and I can never thank them enough for being who they are.

I want to thank the community and friends who I have come to know over the years in New York. My mentor, Dr. Lisa Fortier, has given me guidance, inspired me, and pushed me to always do more. My committee members, Drs. Cornelia Farnum, Moonsoo Jin, Scott Rodeo, and Rebecca Williams helped me to become a better researcher and ultimately develop a unique research niche. I have also had the opportunity to learn from other faculty, including Drs. Lawrence Bonassar, Hussni Mohammed, Itai Cohen, and Warren Zipfel. I have gained so much knowledge and grown professionally from being around such exceptional and talented people.

My friends have had a large impact on my life. Dr. Laura Goodman has been incredibly supportive, both academically and personally, and I can't thank her and her family enough for everything they have done. Dr. Jung Mee Park has provided encouragement and amazing friendship and has taught me resourcefulness, sometimes in the most unexpected places. Natalie Couch is a positive spirit who has always brightened my day and whose words continually inspire me. Laura Kozlowski has shown me how one can get up and keep going, no matter the day. Natalie Kelly has an infectious, upbeat attitude that makes me smile. I would also like to thank the friends who I have made during the years in Ithaca and who have encouraged me, including

Margaret Winter, Nizeet Aguilar, Jim Cunningham, Wisler Charles, Kris Corda and the staff at the Big Red Barn, Dr. Victor Tse, and everyone a part of the Ithaca Triathlon Club, Finger Lakes Running Club, and Finger Lakes Cycling Club. I would also like to thank those who have not only helped me with my research but have been wonderful colleagues and friends, including but not limited to, Jesse Silverberg, Lena Bartell, Dr. Lise Berg, Dr. Ilaria Bronzini, Dr. Robert Bowles, Derin Sevenler, Patrick Satchell, Avtar Singh, Jessica Cross, Rebecca Donnelly, Sarah Poland, Shannon Walsh, Kim McHenry, Dr. Corinne Henak, Jane Park, Dr. Stacie Boswell, Dr. Emily Sundman, Dr. Tim Krebs, Jennifer Puetzer, Brandon Borde, Patrick Burke, Alexandra Scharf, Dr. Heidi Reesink, Mark Riccio, and Dr. Lauren Schnabel.

There are many more people who have touched my life than I can acknowledge on the written page. I appreciate every inspirational story and encouraging word. It has meant more than I can ever express in words, and I will always have gratitude towards those who have been in my life.

TABLE OF CONTENTS

BIOGRAPHICAL SKETCH v

DEDICATION vi

TABLE OF CONTENTS ix

LIST OF FIGURES xii

LIST OF TABLES xiv

LIST OF ABBREVIATIONS xv

LIST OF SYMBOLS xvii

CHAPTER 1 1

Introduction

Osteoarthritis and motivation for cartilage research 1

Post-traumatic osteoarthritis and early cartilage disease 2

Detecting cartilage damage 4

Magnetic Resonance Imaging 6

Computed Tomography 10

Optical coherence tomography 13

Ultrasound 14

Bioelectricity 17

Multiphoton microscopy 19

Conclusion and future directions 21

References 22

CHAPTER 2 30

Identification of cartilage injury using quantitative multiphoton microscopy

ABSTRACT 31

INTRODUCTION 32
METHODS 34
RESULTS 41
DISCUSSION 44
REFERENCES 52
CHAPTER 3 56
Variable responses of cartilage to impact between joints and implications for the development of post traumatic osteoarthritis
INTRODUCTION 58
METHODS 60
RESULTS 66
DISCUSSION 74
REFERENCES 76
CHAPTER 4 80
Hyperoxic treatment after cartilage injury protects against cell death
ABSTRACT 81
INTRODUCTION 82
METHODS 84
RESULTS 88
DISCUSSION 92
REFERENCES 95
CHAPTER 5 98
Discussion, future direction, conclusion
Discussion 98
Future direction 99
Can MPM be adapted for clinical, diagnostic use? 99

Should future cartilage research continued to be performed in one joint? 102

Could oxygen play a role in future PTOA treatment? 103

Conclusion 103

References 104

LIST OF FIGURES

Figure 2.1 35

Schematic of methods.

Figure 2.2 40

Multiphoton microscopy images from a single-image plane within a z-stack, from both control and injured samples.

Figure 2.3 42

Sodium fluorescein and ethidium homodimer-1 validation.

Figure 2.4 43

Percentage of dead chondrocytes after injury, as a function of depth in 50 μm steps, as measured in the sagittal plane.

Figure 2.5 45

3-D reconstructions of control and injured cartilage.

Figure 2.6 46

2-D projections of control and injured cartilage.

Figure 3.1 62

Schematic of methods.

Figure 3.2 67

Exponential decay rate length of cell density in cartilage.

Figure 3.3 69

Distribution of superficial zone chondrocyte profiles.

Figure 3.4 73

Gene expression in control and injured cartilage.

Figure 4.1 85

Schematic of methods.

Figure 4.2 89

Images of control and injured cartilage.

Figure 4.3 91

Chondrocyte viability with normoxic and hyperoxic treatment.

Figure 4.4 93

Hyperoxic treatment minimized chondrocyte death.

LIST OF TABLES

Table 2.1 47

Median peak load (with range), median peak displacement (with range), and median percent-difference between the long- and short-axis (with range).

Table 3.1 65

Primers used for real time quantitative RT-PCR.

Table 3.2 68

Chondrocyte density decay rate length with goodness of fit R^2.

Table 3.3 70

Primers used for real time quantitative RT-PCR.

Table 3.4 72

A multivariate regression analysis was used to determine the effect from injury and joint.

LIST OF ABBREVIATIONS

AGG	Aggrecan
ANOVA/AOV	Analysis of variance
CA	Carpal joint, proximal surface of *os carpale III*
CD-RAP	Cartilage-derived retinoic acid-sensitive protein
COL2A1	Collagen type 2α1 gene
CT	Computed tomography
dGEMRIC	3D delayed gadolinium enhanced MRI of cartilage
DNA	Deoxyribonucleic acid
GAG	Glycosaminoglycan
EL	Elbow joint, *condylus lateralis radii*
FBS	Fetal bovine serum
FP	Patellofemoral joint, *trochlea ossis femoris*
Gd-DTPA^{-2}	Gadolinium diethylenetriamine-pentaacetic acid
HBSS	Hank's balanced salt solution
IGF-I	Insulin-like growth factor I
IL-1β	Interleukin-1β
MC	Metacarpophalangeal joint, *condylus lateralis metacarpi III*
MEM	Minimal essential media
MMP-1	Matrix metalloproteinase-1
MMP-13	Matrix metalloproteinase-13
MPM	Multiphoton microscopy

MRI	Magnetic resonance imaging
MT	Metatarsophalangeal joint, *condylus lateralis metatarsi III*
NIR	Near infrared
OA	Osteoarthritis
OCT	Optical coherence tomography
p (statistics)	p-value
PCR	Polymerase chain reaction
PBS	Phosphate buffered saline
PG	Proteoglycan
PP	Proximal interphalangeal joint, *condylus lateralis phalanx proximalis III*
qPCR	Quantitative polymerase chain reaction
PTOA	Post-traumatic osteoarthritis
SAA	Serum amyloid A
SE	Standard error
SH	Shoulder joint, *caput humeri*
TA	Tarsal joint, distal surface of *os tarsi central*
TPE	Two photon excitation

LIST OF SYMBOLS

2-D	Two dimension
3-D	Three dimension
18S	Ribonucleic acid house-keeper gene
^{23}Na	Sodium isotope
α	Alpha
β	Beta
©	Copyright
°	Degrees
ɣ	Gamma
>	Greater than
≥	Greater than or equal to
<	Less than
≤	Less than or equal to
CO_2	Carbon dioxide
Cp	Gene expression count
fs	Femptoseconds
L-	Levorotatory
ϰ	Kappa
MHz	Megahertz
µg	Microgram
µl	Microliter

μm	Micron
mg	Milligram
ml	Milliliter
mM	Millimolar
MPa	Megapascal
n	Number
ng	Nanogram
nm	Nanometer
ρ	Rho
SYBR	Nucleic acid stain
T	Tesla
T_2	Magnetic resonance imaging measurement (spin-spin)
T2*	Magnetic resonance imaging measurement (spin-spin)
$T_{1\varrho}$	Magnetic resonance imaging measurement (spin-lock)
%	Percentage
±	Plus-minus
x	Times

CHAPTER 1

INTRODUCTION

Osteoarthritis and motivation for cartilage research

Osteoarthritis (OA) is a progressive and degenerative disease that is becoming more prevalent with an increased aging population in the world.[1,2] The etiology of OA is not fully understood and has numerous contributing factors including biomechanical, biochemical, genetic, and nutritional influences.[1,3] However, the initiation of OA begins before clinical signs are observed. Cartilage injury that occurs during adolescence can develop into OA later in life. Cartilage damage, if left undiagnosed and untreated, can silently progress into post-traumatic OA (PTOA), in which clinical signs may not become evident for many years.[4] In order to attenuate this natural disease progression, damage needs to, at minimum, be detected at the early, pre-symptomatic stage of OA. After the disease has become symptomatic and severe, only treatments directed toward symptom management can be applied. Yet, at the early phase, therapeutic or rehabilitative methods could be administered to minimize the progression of OA. However, current clinical imaging techniques are limited in their resolution and may underdiagnose small focal regions of cartilage damage.[5,6] With improved detection of cartilage damage, diseased cartilage can be identified earlier, which will strengthen the knowledge of the pathogenesis of PTOA and facilitate the development of new OA treatments.

Cell death occurs immediately after injury,[7,8] and the importance of understanding how injury and cell death may lead to the progression of PTOA is becoming more apparent.[9] In this dissertation research, high resolution imaging was used to help characterize the changes within equine or bovine cartilage immediately after injury. Using equine and bovine injury models can help improve understanding

in human OA because both animals have naturally-occurring OA that is similar to that found in humans. Multiphoton and confocal microscopy were used to identify cell death and the distribution of cells and cell death. Cell death along matrix cracks was quantified. This concept was further examined because cells adjacent to the cracks may be exposed to higher concentrations of oxygen post-injury than pre-injury. Oxygen exposure can affect the magnitude of cell death after injury.

The overall motivation for the dissertation research was to identify a microscopic technique to identify early, subclinical cartilage damage *ex vivo* that could be applied clinically to expand the understanding of cartilage trauma. The hypothesis for the dissertation was that the use of high resolution microscopy imaging would identify differences in cartilage damage within joints, between joints, and between high and low oxygen exposure after traumatic injury.

Post-traumatic osteoarthritis and early cartilage disease

Trauma or repetitive injurious activity can result in permanent damage to cartilage.[7,8] With time, trauma-related damage may play a role and increase the risk in the progression of cartilage degeneration, eventually resulting in PTOA. In a 36 year long study following young adults (mean age at enrollment=22 years), there was increased association in the development of PTOA by the age of 65 with individuals who reported experiencing a knee injury prior to enrollment (13.9%) over those who did not (6.0%).[4] This suggests that experiencing a joint injury early in life may increase the risk of developing PTOA with age. Yet despite this increased association of PTOA, acute injuries might not be treated appropriately with PTOA in mind,[4] putting many adults at risk for developing PTOA. It is estimated that 5.6 million Americans are affected by PTOA, with 12% of OA cases being attributed to PTOA.[10] The financial impact of PTOA is large, with an associated economic cost of almost $12

billion (US dollars).[10] PTOA is a widespread problem that many adults will experience, although many patients and physicians may not appreciate the increased risk.

PTOA can progress undiagnosed for years because subtle changes and degeneration in cartilage can occur while the joint remains grossly normal. After prolonged, long-distance running, changes in the orientation of the superficial zone collagen can be detected by polarized light microscopy of histological sections of cartilage. However, cartilage thickness, total collagen, and gross appearance do not change.[11] This suggests that subtle structural changes might not be detected during typical evaluation of cartilage degeneration, particularly during visual (arthroscopic) examinations. Physical examination may also underdiagnose PTOA. In an experimental PTOA model in horses, initial lameness decreased after 1-2 months,[12] suggesting that in traumatic injuries, only a small period of time may exist to clinically detect pain during the initial inflammation stage. After the initial 1-2 month inflammatory stage, cartilage damage may no longer elicit enough clinical symptoms for the patient to seek healthcare. After this inflammatory period, diagnosis may become more difficult. Synovial fluid biomarkers may or may not be useful in the early stages of PTOA. Sulfated glycosaminoglycan (GAG) concentration is not significantly affected but cartilage oligomeric matrix protein levels are increased in metacarpophalangeal joint synovial fluid within eight months of mechanical trauma to cartilage.[12]

Detecting cartilage injury is challenging. It may not be possible to detect cartilage damage radiographically within the first year of injury onset without comparing radiographs from post-injury to pre-injury.[12] However, normal baseline radiographs may not pre-exist for an injured joint. While significant changes in radiographic evidence can be found when comparing the same pre- and post-impact

site, there is no significant radiographic difference between control and injured limbs 8 months after trauma.[12] Consequently, it may take several years for PTOA to develop after sustaining an injury. In a 36 year follow-up study, adults who had reported experiencing a knee injury prior to study enrollment were found to experience clinical symptoms of OA within 22 years (standard deviation=13 years) of enrollment.[4] If cartilage damage is initiated at the time of joint injury, it may be difficult to diagnose in the early stages, which results in an increased risk of PTOA.

Detecting cartilage damage

There are currently no treatments that can return degraded cartilage to its normal, native state. Therefore, cartilage damage must be treated early to delay the progression to OA. In order to treat or modify the progression of early OA, degeneration or damage must be identified early. Cartilage is routinely evaluated during surgical procedures using an arthroscopic camera that provides optical magnification. Arthroscopic cameras provide greater details to a surgeon than the unaided eye. However, during arthroscopy, identifying early disease and determining the severity of disease is a qualitative process, and only the surface of the cartilage can be evaluated. Of over 31,000 arthroscopies performed in 1991-1995, chondral lesions were identified in 63% of the procedures, with almost 10% of the identified lesions being described as low grade—or, having softening of the cartilage.[13] Low grade lesions can be challenging to diagnose with an arthroscopic camera, particularly in defining the border or depth of degradation. Of 105 experienced arthroscopists, most (61%) surgeons felt that differentiating normal and low-grade cartilage disease during arthroscopies was simple, 12% reported that differentiating normal and low grade was poor, and 22% reported that there is a need for improved differentiation.[14] Not being able to clearly identify or define the extent of damage with small lesions may result in

inadequate treatment.

Physicians would be able to more readily provide effective treatments to patients by having the ability to objectively evaluate cartilage integrity. There is a need for advanced technology to accomplish this objective. An overwhelming majority (75%) of surgeons reported that being able to use an objective measurement during surgery would be very or somewhat useful.[14] If such an instrument were available, 88% of surveyed surgeons would use it: 16% reported that they would use it every time, and 72% would use it in questionable cases.[14] In addition, an objective measurement during arthroscopic examination could be utilized when the primary pathology is not a cartilage lesion. Almost 40% of primarily pathologies found during knee arthroscopies in young adults between the ages of 20 and 30 were ACL injuries.[13] In such cases where cartilage damage may not be the primary injury, a highly resolved, objective instrument may help to identify secondary cartilage injury. An objective, quantifiable measurement could help to determine the boundary of a non-distinct lesion, the integrity of cartilage bordering a distinct lesion, and the presence of secondary cartilage damage that may have occurred during a different primary injury, such as a ligament tear.

Recent and developing improvements in cartilage imaging can make detailed evaluation of cartilage possible by providing quantifiable measurements. The three non-invasive clinical modalities most often used to diagnose cartilage disease are: radiography, magnetic resonance imaging (MRI), and computed tomography (CT). Radiographs are most often used first as a screening method. However, radiographs cannot be used to characterize changes with cartilage and instead are commonly used to identify osteophytes associated with late-stage OA. MRI and CT can be used to diagnose changes within the cartilage. However, they are currently limited in their resolution, failing to identify small regions of damage that could be the most useful in

early stage diagnosis. MRI and CT are more likely to underdiagnose than overdiagnose cartilage defects.[5,6] Future advancements will improve MRI and CT capabilities in detecting early damage, such as with improved contrast agents and instrumentation. *In vivo* or arthroscopic imaging that is also being developed has higher resolution capabilities than MRI and CT and can provide additional, unique biological information. These *in vivo* techniques include optical coherence tomography (OCT), ultrasound imaging, bioelectricity including both streaming potential measurement and non-invasive electroarthrography (EAG), and multiphoton microscopy (MPM). These techniques all provide high detailed information about cartilage structure, which can sustain subtle changes that are not grossly apparent.[11]

Magnetic Resonance Imaging

MRI is a widely accepted, *ex vivo* imaging technique that can be used to quantify cartilage extracellular matrix and identify changes in the matrix associated with early OA. Traditionally, radiographic measurement of joint space width (JSW) has been used for diagnosing cartilage degradation, with decreased JSW presumably correlating with thinning cartilage. By using similar correlative measures, MRI can detect increased hydration that occurs during cartilage degeneration. While both methods indirectly diagnose cartilage degeneration, MRI quantification of cartilage thickness is more sensitive in identifying changes within the knee than radiograph quantification of JSW.[15] MRI can detect cartilage degeneration early: using T2* values, degenerative cartilage has been identified at 4 weeks after anterior cruciate ligament transection in rats with 4.7T MRI.[16]

MRI works by exciting and then detecting the relaxation time of proton spin, from excited state back to steady state. The location of the protons being detected is typically in unbound, water in cartilage. Proton MRI sequences in cartilage include T_2

(spin-spin) weighted relaxation for indirectly measuring collagen quantity[17] and orientation,[18] T2* (spin-spin in inhomogeneous magnetic field[19]) to evaluate collagen,[20] $T_{1\rho}$ (spin-lock) weighted relaxation for indirectly measuring proteoglycan quantity,[17,21,22] contrast enhanced detection with gadolinium to measure GAG quantity,[23] and magnetization transfer. Sodium can also be utilized for MRI to directly quantify proteoglycan concentration.[24,25]

3T MRI has become standard for diagnosing cartilage injury. When comprehensive knee MRI scans are used and followed by arthroscopic procedure, both 3T and 1.5T MRI can resolve cartilage lesions. However, 3T has an advantage over the weaker-field 1.5T MRI, with increased agreement between independent readers, less false-negatives for detecting lesions in 3T (9%) than 1.5T (12%), and higher sensitivity for detecting lesions in 3T (69%) than 1.5T of (60%) with multiplanar turbo spin-echo sequence.[26] Sensitivity of 3T MRI in detecting lesions can be further increased by 14% with the addition of T_2 mapping sequence.[27] MRI signal is correlated with cartilage degeneration identified by biochemical, histological, and arthroscopic methods. T_2 and $T_{1\rho}$ weighted-sequence measurements acquired with 3T are present in the same regions of cartilage with increased matrix metalloproteinase activity and decreased cellularity.[22] This suggests that MRI may identify regions with altered biological activity.

MRI can also help detect the progression of cartilage degeneration over time. When lesions are monitored longitudinally for 3 years, T_2 and $T_{1\rho}$ signals increase over time, presumably as the lesions worsen.[28] The use of contrast agents also increases the capabilities of 3T MRI to resolve cartilage degeneration. With the use of the negatively charged contrast agent gadolinium diethylenetriaminepentacetate (Gd-DTPA; gadopentetate), 3D delayed gadolinium enhanced MRI of cartilage (dGEMRIC) provides an inverse relationship of GAG concentration[23] that is highly

reproducible (intraclass correlation 0.87-0.95) when reimaging the same early OA knee.[29] Overall, 3T MRI still fails to identify small or early lesions. MRI images read by trained radiologists as normal that were later identified as false-negative were most commonly classified as Noyes grade 1 during arthroscopy.[5] This suggests that early OA can be missed with 3T scanning and that higher resolution scanning is necessary for these early stage cases.

MRI at 7T has improved spatial resolution and shorter scan duration over 3T scanning due to the signal-to-noise (SNR) ratio of 7T being, in theory, 2.3 times higher than at 3T.[30] Spatial resolution of 7T in human knee and hip has been demonstrated at ~200 μm x 200 μm x 1 mm to identify early cartilage changes.[31,32] This high voxel resolution can be particularly important to yield high details in other joints with thinner cartilage, such as the ankle. T_1-weighted gradient echo sequences can be collected in one-third of the scan time with 7T than with 3T,[30] which is beneficial in minimizing artifacts resulting from patient movement. In practice, the SNR improvement in 7T over 3T is dependent on the unique scan sequence, with an improvement of 86.7% in 2D PD-weighted fat-saturated fast spin echo and 60% in 3D T_1-weighted gradient echo found when scanning human ankles. However, decreased performance in SNR of 25% was found with 2D T_1 weighted spin echo, which may have been due to T_1-weighted optimization.[33] These varying SNRs suggest that results are highly sensitive to coil and protocol parameters. Commercially available coils for 7T MRI scanning are limited mostly to proton knee coils, with in-house coils used to successfully scan deep tissue such as the hip with high resolution.[32] The future clinical application and development of 7T proton and ^{23}Na MRI may ultimately be hindered by the commercial availability of scan coils and subsequently protocol development. These similar deterrents were also historically present for 3T MRI, which is now standard of care in many radiology departments.

Non-proton ^{23}Na 7T MRI[34,35] is also being used to detect early cartilage degradation by measuring the change in concentration of ^{23}Na associated with GAG loss.[24,25] ^{23}Na has a high correlation with GAG concentration; however, ^{23}Na MRI acquisition times can be long (>15 minutes). Techniques including compressed sensing by under-sampling k-space have been investigated to shorten scan duration.[35] ^{23}Na MRI may be a tool for diagnosing early cartilage degeneration, but this MRI technique still needs further development to provide higher resolution and faster scan times before being feasible for routine clinical use.

MRI has limitations. In-plane resolution is limited, making the imaging of early changes difficult, particularly in thin cartilage. In a systematic review, MRI was found to be accurate in detecting patellar (84%) and trochlear (83%) defects, but most traditional MRI sequences tend to underdiagnose, rather than overdiagnose, defects.[6] In joints where cartilage is less than 500 μm in thickness, early OA may involve only a fraction of the tissue. Even with 7T MRI single plane resolution of 200 μm, sites of early OA may be a fraction of this spatial sampling site and be missed. An ultra-high field, full body 11.7T MRI scanner is being developed for high resolution brain imaging, with reported a single plane resolution of 100 μm.[36,37] This scanning method could provide improved detection of cartilage damage. Safety concerns will need to be addressed at this high field strength, especially with reporting of altered cognitive function resulting from magnetic stray fields near 7T scanners.[38] A second limitation is that MRI typically measures proton relaxation in unbound water. These measurements may be affected by both macromolecule concentration and alignment, leading to relaxation times that may be attributed to solely matrix concentration. T_2 mapping cannot be used alone without additional scan sequences due to the potential effect of collagen degradation on T_2 mapping values.[27] However, contrast enhanced MRI such as dGEMRIC, dual gadopentatate and Mineric (trace element replenisher)

T_1 and T_2 sequencing,[39] non-proton ^{23}Na MRI, and magnetization transfer sequences, which rely on both unbound and bound water, may help to improve this particular limitation. Cartilage thickness measurements in MRI can be affected by joint loading prior to scanning. T_2 weighted values in defects are higher in unloaded cartilage than cartilage that has been loaded prior to scanning.[40] Patient activity prior to MRI scanning can create a potential confounding factor on measured cartilage thickness emphasizing the need of a standardized protocol for physical activity prior to scanning to minimize this effect. Lastly, the commercial availability of coils and protocol sequences may slow the progression of high resolution MRI. This limitation occurs for any new technological advancement and can be said for any method discussed herein.

Computed Tomography

Cartilage can be visualized with non-invasive CT. Multiple image slices and three-dimensional reconstructions are created by computer-processing of x-rays, which yield detailed information about deep tissue. Using soft tissue kernel-based CT with post-processing, CT can be used to identify regions of different thickness of articular cartilage within the human shoulder, with results similar to those found with MRI or anatomical sections.[41] However, fine details of cartilage needed to identify early OA are not easily visualized with standard soft tissue CT imaging. Contrast agents and acquisition methods have made it possible to achieve high details of cartilage that correlate with MRI. When a combination of ioxaglate and gadopentetate is used with CT and the same ioxaglate-gadopentetate combination or solely gadopentetate is used with MRI, CT and MRI findings of cartilage strongly correlate (R=0.65).[42] This suggests that either imaging modality could be used to detect cartilage disease, which is beneficial to facilities that have limited equipment resources.

Contrast agents are commonly used during CT imaging of cartilage. Clinical

contrast agents are typically anionic and either iodine (e.g., ioxaglate) or gadolinium (e.g., gadopentetate, also used in MRI) based. Iodine and gadolinium contrast agents can be readily visualized with CT. Contrast agents work by being excluded from or attracted to the cartilage matrix. GAGs are negatively charged and repel anionic dyes and attract cationic dyes. Imaging with anionic contrast dyes is achieved because anionic dyes are concentrated in regions with little GAG such as in the synovial fluid and lesions, or alternatively, by being excluded from regions that are dense with GAGs such as normal cartilage. Healthy cartilage will have less anionic dye present than diseased cartilage that is depleted of GAGs. CT scanning with anionic, iodine-based contrast dyes has been reported to both highly correlate (anionic tri-iodinated dye, R^2=0.83[43]) or poorly correlate (ioxaglate, R^2=0.2,[44] R=-0.64[45]) with biochemically measured GAG content by dimethylmethylene blue (DMMB) assay[43,44] or safranin-O-staining.[45] Different types of anionic iodinated dyes, levels of degradation, and lengths of dye incubation can contribute to differing results of CT imaging. Optimizing the methods for *in vivo* dye incubation could help the dye and GAG correlation, and subsequently, clinical diagnosis. Ioxaglate can detect small cartilage injuries in as little as 3 hours after trauma;[46] however, anionic dyes take over 29 hours for diffusion to reach near-equilibrium state.[47] Cartilage injury can be detected in almost a tenth of the time needed for dye to reach the diffusion equilibrium within cartilage, but the accuracy of quantifying the severity of injury may be limited with a 3 hour incubation. In addition, ioxaglate does not cross the bone-cartilage interface,[45] suggesting that intra-articular injection may be more effective than intravenous injection.

The use of CT with cationic contrast dyes provides a solution to the limitations with anionic dye exlcusion. Cationic dyes have a direct correlation with negatively charged GAGs. Cationic dyes like CA4+ have a higher correlation with GAG (R^2=0.83) than negatively charged dyes (ioxaglate R^2=0.2; gadopentetate R^2=0.22).[44]

Further development is necessary to help achieve detailed imaging of cartilage with anionic and cationic dyes that have high correlation to matrix biochemical properties.

Cartilage can be imaged using CT without contrast agents with new acquisition methods. Normal and OA human patellar cartilage can be identified with phase contrast imaging (PCI) X-ray CT (PCI-CT). In PCI-CT, a highly collimated X-ray beam is delivered to the sample, and emerging, refracted, and scattered radiation is collected and converted to visible light. These data are analyzed to determine an apparent "pattern" or "texture" of the matrix and the distribution of chondrocytes. While this method is being tested with *ex vivo* samples, it may have a future role with adaptation for detecting small matrix defects, with its high resolution of 8 μm x 8 μm per pixel.[48] Use of the highly collimated X-ray beam in a synchrotron facility will need to be adapted for clinical use and safety.

CT resolution has been further improved to micron resolution. μCT can provide higher resolution imaging for *ex vivo* samples or *in vivo* imaging of small specimens. μCT has a resolution of 25 – 85 μm^3 voxels, with some μCT systems having the capability to go lower.[44,49] These instruments often have a small bore for the sample, due to the set up of detectors. This limits μCT potential to use for smaller applications, such as the hand or ankle. Further clinical research would be needed to determine the safety of using μCT with patients, but equipment and acquisition techniques could reduce μCT radiation exposure to similar levels of current clinical CT.[50]

CT has similar potential and limitations as MRI. CT can detect early cartilage degeneration but is less able to identify small cartilage lesions. CT and MRI are more effective than radiographs and are useful instrumentation for initial diagnosis, prior to arthroscopic procedures. PCI-CT and μCT may both be able to provide great details about cartilage disease, but further development needs to be performed prior to clinical

application. If PCI-CT and higher resolution μCT can be combined with contrast agents for clinical use, this tool could be extremely functional for non-invasive cartilage evaluation.

Optical coherence tomography

OCT provides, in general, a cross sectional view of cartilage from an arthroscopic or open-joint approach. This imaging technique is achieved by collecting the back-scattering of infrared light, which provides deep penetration of tissue to reveal subsurface defects.[51] Using OCT, the integrity of the cartilage collagen matrix can be assessed, the thickness of cartilage can be measured, and the bone-cartilage interface can be evaluated.

A hand-held OCT probe[52] can be inserted arthroscopically, such as through a 0.9 mm portal, or smaller for a less invasive, non-surgical technique.[53] OCT has an in-plane resolution of about 10 μm[53,54] and depth penetration of up to about 1.5 mm[55] to visualize thinning, fibrillation, and birefringence. Modified Mankin scoring of OCT optical sections and histological slide sections have a high agreement (κ=0.80),[51] suggesting that OCT can serve as an effective method to assess deeper tissue that cannot be seen with a standard arthroscopy lens. OCT signal intensity and edge variance correlates with 313 μm x 313 μm resolution, T_2 mapping in MRI.[55]

Using different evaluation methods, including ICRS lesion scoring parameters,[53] OCT roughness index (ORI),[56,57] optical surface reflection coefficient (ORC),[56,57] variation of surface reflection (VSR),[57] and optical backscattering (OBS),[57] cartilage degradation can be quantified. ICRS scoring with OCT can provide an overall assessment of cartilage disease but has only moderate correlation with standard arthroscopy (R=0.503).[53] ORI, ORC, VSR, and OBS can be used to detect cartilage injury caused by mechanical trauma.[57] ORI and ORC decrease in bovine

cartilage treated with collagenase but not trypsin, suggesting OCT may be more sensitive to changes in collagen than GAG.[56] This is not surprising because OCT relies on reflection, and collagen is reflective, unlike GAGs.

OCT has the resolution to differentiate cartilage zones due to the different refractive indices (RI) among zones.[58] However, different RIs have been reported between species in the literature,[58,59] which can affect cartilage depth measurements. This suggests that optimization of imaging parameters may need to be outlined prior to evaluating the images of cartilage. Furthermore, when acquiring OCT images, if the probe is not perpendicular to the surface, ORI, ORC, VSR, and OBS can be affected.[57] OCT has an in-plane resolution of about 10 μm, which is about the size of one cell. However, OCT cannot discern cellular viability or morphology. The inability of OCT to provide biological details is a disadvantage shared with MRI and CT. No *in vivo* clinical imaging techniques can provide cellular level details, and much of the information concluded about the "health" of cartilage is based on matrix structural changes.

Ultrasound

Ultrasound imaging of cartilage is acquired by collecting the echoes of pulsed, high frequency sound waves that are transmitted externally to the joint or arthroscopically to the cartilage. The transmitted and collected sound waves will be different from each other, after interacting with a surface or tissue. Sound waves can be attenuated (reduced amplitude and intensity) by reflection, scattering, and absorption; or refracted (altered direction and velocity). Interaction with different tissue—whether it is bone or cartilage, or healthy or diseased tissue—will cause different attenuation or refraction of sound waves, which can be used to characterize the properties of the tissue. In arthroscopic surgery, this information can provide

details about the integrity of cartilage matrix to a greater depth than can be visualized with an arthroscopic lens, allowing previously unidentified lesions to be diagnosed and treated.

Non-invasive ultrasound can be used to identify OA. The axial resolution of non-invasive ultrasound is <1.0 mm at 13 MHz,[60] providing gross details of cartilage and bone. Non-invasive ultrasound is moderately correlated with both *in vitro* ultrasound and histological findings (Spearman ρ=0.41-44 and 0.39-0.44, respectively).[61] In the knee, scoring cartilage degeneration by non-invasive ultrasound correlates with the same adapted Noyes' scoring system performed with an arthroscopic camera. Correlation of ultrasound and arthroscopy is site dependent in the knee, with the femoral sulcus (R=0.593) and medial femoral condyle (R=0.465) being moderately correlated, but the lateral femoral condyle (R=0.262) having non-significant correlation.[60]

Arthroscopic ultrasonographic imaging can provide greater details than external ultrasound and help visualize areas not possible with external ultrasound, such as under the patella in the knee. Several measurement parameters can be used for arthroscopic or *in vitro* ultrasonographic imaging. Ultrasonic reflection coefficient (R),[62,63] integrated reflection coefficient (IRC),[64] ultrasonic roughness index (URI),[64] apparent integrated backscattering coefficient (AIB),[64] wave echo,[65,66] and wave magnitude and velocity[65,66] have all been reported in the evaluation of cartilage. R, IRC, and AIB show low coefficient of variation when imaging different cartilage sites, whereas URI is more variable.[64] Wave echo duration and magnitude are similar among joints, such as knee and ankle, when evaluating healthy cartilage.[66]

Arthroscopic and *in vitro* ultrasonography can be performed using low (~10 MHz) or high (20-50 MHz) frequency wavelengths. Lower frequencies allow for deeper imaging than higher frequencies but have lower resolution images than higher

frequencies can provide. Low frequency ultrasonography can be used to visualize both cartilage and bone, whereas high frequency can provide greater details of the surface. Using low 9 MHz frequency that can penetrate to the subchondral bone, R, IRC, URI, and AIB can be used to discern the cartilage-bone interface, making the measurement of cartilage thickness possible.[64] With 9 MHz frequency, reflection coefficients R and IRC can be used to identify natural cartilage disease, and these measurements correlate with histological Mankin scoring (R>0.56). Neither URI, with its high variability, nor AIB significantly correlates with histological evaluation,[64] suggesting that R and IRC may be better parameters than URI or AIB for grading cartilage degeneration at low frequency. Wave echo duration and magnitude measurements can resolve cartilage lesions when using lower resolution 10 MHz frequency.[66]

Higher frequency sound waves such as 20-50 MHz can help capture greater details of cartilage during arthroscopic or *in vitro* imaging but at the loss of imaging deep tissue. The axial resolution of 20 MHz ultrasound has been reported to be 60 μm[63] and 30 μm at 50 MHz.[67] High frequency ultrasound of 40 MHz can still be used to visualize the cartilage-bone interface in sites of thinner cartilage, up to ~1.65 mm.[68] Surface roughness[62,63,68] and degradation[63,68,69] can be visualized at this resolution. Using *in vitro* 20 MHz ultrasound, reflection coefficients R and IRC decrease and URI increases after either mechanical surface abrasion[63] or collagenase treatment,[63,65] suggesting that these measurements could identify cartilage matrix that has structural damage. In cartilage treated with chondroitinase, R, IRC, and URI are not significantly different,[63] indicating that these measurements do not identify GAG loss. Instead, a new echo pattern or altered sound velocity can be used to resolve the edge of chondrointinase degradation and subsequent GAG loss.[65] The depth of cartilage degeneration that results from trypsin degradation can be measured using 50 MHz ultrasound, which significantly correlates to histological measurements (R^2≥0.63).[69]

The depth of degeneration quantified with ultrasonography, however, tended to be less than the depth that was quantified with histological sections,[69] suggesting that ultrasonography may be generally limited in detecting GAG loss.

Ultrasonographic imaging can be adapted for arthroscopic procedures using a 1 mm diameter instrument. R, IRC, AIB have a high correlation with ICRS grading performed during arthroscopic examination (R=0.939), with differences being skewed toward more severe scoring by ultrasonography.[68] This moderate difference is likely due to the ability of ultrasound to discern degradation below the surface. R and IRC are decreased and URI is increased in both mechanically damaged cartilage[70] and naturally occurring fibrillated cartilage.[68]

Ultrasonography has similar potential applications and limitations as OCT. Non-invasive ultrasonography may be a potential screening method to replace or compliment radiograph screening. Current investigations of the optimization of acquisition parameters for different diagnostic applications will help to improve ultrasonography use for cartilage evaluation in the clinic.

Bioelectricity

Cartilage degeneration can be evaluated by capitalizing on its bioelectrical properties. Streaming potential due to positively-charged sodium ions and negatively-charged GAGs[71,72] or bulk electrical impedance due to water content[73] can be used to assess the integrity of cartilage, which can be graded with both non-invasive, external methods and *in vivo* methods.

By loading and unloading the knee, fluid flow generates a flux of sodium ions that creates a streaming potential that can be measured both non-invasively and *in vivo*. Streaming potential can be detected with EAG, where electrodes are placed on the skin near the joint line.[72] Significantly different streaming potentials can be

detected between normal and OA knees using EAG. However, repeatability of measurements within a normal knee is site dependent, with some sites closer to the joint line being more consistent than those farther from the joint line.[72] Site dependency could affect results when evaluating a joint for disease, particularly if the test is performed by different clinicians. The potential diagnosis of OA using non-invasive streaming potential by EAG is promising, particularly among other developing cartilage techniques that require invasive procedures. EAG may be effective for initial OA screening as a diagnostic tool that is directly reflective of cartilage degeneration, unlike radiographs. The relatively low resolution of EAG makes it inappropriate for fine-tuned diagnostics. Improved repeatability and adaptation for other joints need to be addressed prior to clinical application.

Electrical streaming potential can also be measured arthroscopically. Measurements of the electrical streaming potential *in vitro* and *in vivo* are sensitive and can detect changes in the matrix after enzymatic degradation, including by chondroitinase or trypsin,[74] and mechanical injury.[75] The streaming potential integral (SPI) can be measured by indenting the cartilage surface with an arthroscopically-designed probe. SPI has been shown to correlate with ICRS and Mankin scores (R=-0.749 and -0.409, respectively).[76] SPI measurements are significantly different between normal cartilage and moderately to severely mechanically-injured cartilage resulting from 28-49 MPa loading.[75] The logarithm of SPI also correlates with cartilage thickness (R=-0.496), suggesting that it may be applied clinically for determining the differences in site-to-site cartilage-bone interfaces.[76] SPI has a high intraclass correlation between repeated measurements by different users (ICC=0.861).[75] However, the sensitivity of SPI is limited and fails to detect a significant difference between normal cartilage and mild injuries created by 17 MPa loading.[75] SPI may be able to compliment an arthroscopic examination by providing

details of deeper cartilage, but it might be limited in the additional information it can provide. By improving the sensitivity of *in vivo* SPI measurement, this high inter- and intra-user repeatable technique could be a promising tool to compliment current arthroscopic imaging.

The electrical impedance, a characteristic of the bulk electrical property of cartilage, can be measured *ex vivo* to detect degraded cartilage. Unlike streaming potential that is dependent on the local cartilage properties, electrical impedance is dependent on the bulk of the tissue. In an *ex vivo* setting, a cartilage explant is placed between two electrodes, and a voltage is applied to measure impedance. Impedance in cartilage is dependent on the permeability of cartilage to water, and this permeability changes when cartilage is degraded. The electrical resistivity significantly decreases after hyaluronidase or collagenase treatment, and the amplitude of change is dependent on the duration of treatment with enzymes.[73] This concept has potential to be used in a clinical setting to diagnose altered matrix integrity. This method needs further development before it can be adapted to *in vivo* use.[73]

Multiphoton microscopy

Cartilage damage can be visualized at the cellular level using MPM.[77,78] MPM is a microscopy technique that uses pulsed, infrared photons to acquire sub-micron[79] images of intact, live tissue to approximately two hundred microns in z-depth.[80] MPM images are gathered by utilizing both the backscattering of excitation photons in the nonlinear optical process called second harmonic generation (SHG) and the two-photon excitation of both autofluorescent molecules within unstained tissue and fluorescent dyes added to tissue. MPM images can be acquired from intact and unstained tissue, providing cellular resolution with great z-depth that is not available with other microscopic, *in vivo*, or non-invasive imaging techniques.

Cartilage extracellular matrix can be visualized using both SHG and autofluorescence. Collagen in cartilage matrix has a strong SHG emission,[81] which can be used to identify and quantify cartilage damage. Quantification of SHG detects differences in collagen content between normal and repair cartilage and correlates with polarized light microscopy (R=-0.76).[78] When cartilage is subjected to freezing to create structural changes in collagen, SHG intensities become diminished.[82] However, unlike immuno-staining and polarized light microscopy techniques that require sample processing, SHG with MPM can be used to evaluate matrix collagen in live, intact cartilage samples. Cartilage matrix also contains molecules like elastin[83] that autofluoresce to provide information about extracellular and pericellular matrix.[79] Individual elastin fibers, elastin fiber branching, and diffuse pericellular elastin can be resolved with MPM.[83] Disruption of the elastin fiber network could be used to identify regions of cartilage damage. Diminished pericellular elastin autofluorescence could be a potential tool to indicate compromised chondrocytes. Fine details of the cartilage matrix integrity can be evaluated when SHG and autofluorescence are combined, including cracks as small as 2 μm that result from mechanical trauma.[77] This type of small structural damage that can be identified with MPM is undetectable with other *in vivo* imaging techniques.

MPM can resolve damaged regions of cartilage through the use of dead cell stains[77] and evaluation of matrix diffusivity.[84] Individual cells can be identified to determine specific regions of increased cell death, such as near matrix cracks that are below the resolution of previously discussed imaging techniques.[77] MPM can also be used to monitor cartilage matrix diffusivity, or the diffusion and flow of molecules in cartilage.[84] This technique could identify regions of diseased cartilage, where diffusion may be altered from either changes in GAG concentration or structural loss of matrix integrity such as cracking. The ability to detect changes in cell viability and changes

within the cartilage matrix by cell diffusive properties would aide in the diagnosis of diseased cartilage.

MPM has not been used clinically to evaluate cartilage, but recent work in other medical fields[85-88] and in *ex vivo* studies[82, 84] suggests that MPM has potential as a diagnostic tool. MPM imaging is being investigated in the oncology field because of its ability to resolve differences between normal and cancerous skin and lung tissue.[85—88] The potential of MPM in the medical field is being realized because it can detect differences between normal and abnormal tissue, particularly in early stage disease before abnormalities are detectable with other imaging modalities. MPM can be used to identify small (<2 μm) regions of injury in cartilage in an *ex vivo* setting[77] but will require adaptation before it can be used clinically. With clinical adaptation, small cartilage damage can be detected to aide in early treatment and mitigation of PTOA progression. High resolution longitudinal studies that have not previously been possible could be performed with arthroscopic MPM to help determine the minimal threshold of damage that degenerates into PTOA and evaluate corresponding therapeutic targets.

Conclusion and future directions

Identifying and understanding changes in cartilage immediately after injury will benefit patients both directly in the clinic and indirectly through the advancement of PTOA treatments. Current clinical imaging modalities MRI and CT do not provide resolution that is high enough to identify small cartilage injuries. While OCT, ultrasound, and electric streaming potential provide increased resolution over MRI and CT, they do not have the submicron resolution or cellular detail that MPM provides.

With clinical adaption, MPM could be used during arthroscopies to define the border of damaged and healthy tissue near a lesion, to provide cellular and structural

details of a low grade cartilage damage, and to evaluate regions of cartilage that may have received trauma during an injury such as an anterior cruciate ligament tear. While the application of MPM is broad, it would most likely be used during cases where an arthroscopy was recommended based on physical exam and MRI or CT imaging. It is unlikely that a patient would be referred for arthroscopic MPM simply because of traumatic injury, and instead MPM would be used to compliment the pre-operative diagnosis and arthroscopic examination. The complimentary imaging can help detect small damage so that early treatment can be provided to mitigate further damage and development of PTOA. Use of MPM to identify optical biomarkers might lead to the discovery of PTOA chemical biomarkers that could be detected in blood or urine tests to monitor the presence or progression of PTOA and response to therapeutic intervention.

References

1. Felson DT, Lawrence RC, Dieppe PA, et al. 2000. Osteoarthritis: New insights. part 1: The disease and its risk factors. Ann Intern Med 133: 635.

2. Woolf AD, Pfleger B. 2003. Burden of major musculoskeletal conditions. Bull World Health Organ 81: 646-656.

3. Borrelli Jr J, Silva MJ, Zaegel MA, Franz C, Sandell LJ. 2009. Single high-energy impact load causes posttraumatic OA in young rabbits via a decrease in cellular metabolism. J Ortho Res 27: 347-352.

4. Gelber AC, Hochberg MC, Mead LA, et al. 2000. Joint injury in young adults and risk for subsequent knee and hip osteoarthritis. Ann Intern Med 133: 321-328.

5. Van Dyck P, Kenis C, Lambrecht V, et al. 2013. Direct comparison of MR imaging at 1.5-and 3.0-T for evaluating the articular cartilage of the knee. 4: S255-S255.

6. Harris JD, Brophy RH, Jia G, et al. 2012. Sensitivity of magnetic resonance imaging for detection of patellofemoral articular cartilage defects. Arthroscopy: The Journal of Arthroscopic & Related Surgery .

7. Natoli RM, Scott CC, Athanasiou KA. 2008. Temporal effects of impact on articular cartilage cell death, gene expression, matrix biochemistry, and biomechanics. Ann Biomed Eng 36: 780-792.

8. Sauter E, Buckwalter JA, McKinley TO, Martin JA. 2012. Cytoskeletal dissolution blocks oxidant release and cell death in injured cartilage. J Orthop Res 30: 593-598.

9. Anderson DD, Chubinskaya S, Guilak F, et al. 2011. Post-traumatic osteoarthritis: Improved understanding and opportunities for early intervention. J Orthop Res 29: 802-809.

10. Brown TD, Johnston RC, Saltzman CL, Marsh JL, Buckwalter JA. 2006. Posttraumatic osteoarthritis: A first estimate of incidence, prevalence, and burden of disease. J Orthop Trauma 20: 739-744.

11. Arokoski J, Hyttinen MM, Lapveteläinen T, et al. 1996. Decreased birefringence of the superficial zone collagen network in the canine knee (stifle) articular cartilage after long distance running training, detected by quantitative polarised light microscopy. Ann Rheum Dis 55: 253-264.

12. Rickey EJ, Cruz AM, Trout DR, McEwen BJ, Hurtig MB. 2012. Evaluation of experimental impact injury for inducing post-traumatic osteoarthritis in the metacarpophalangeal joints of horses. Am J Vet Res 73: 1540-1552.

13. Curl WW, Krome J, Gordon ES, et al. 1997. Cartilage injuries: A review of 31,516 knee arthroscopies. Arthroscopy: The Journal of Arthroscopic & Related Surgery 13: 456-460.

14. Spahn G, Klinger HM, Hofmann GO. 2009. How valid is the arthroscopic diagnosis of cartilage lesions? results of an opinion survey among highly experienced arthroscopic surgeons. Arch Orthop Trauma Surg 129: 1117-1121.

15. Cotofana S, Buck R, Dreher D, et al. 2013. Longitudinal (1-year) change in cartilage thickness in knees with early knee osteoarthritis: A within-person between-knee comparison-data from the OAI. Arthritis care & research .

16. Tsai P, Lee H, Siow TY, et al. 2013. Sequential change in T2* values of cartilage, meniscus, and subchondral bone marrow in a rat model of knee osteoarthritis. PloS one 8: e76658.

17. Duvvuri U, Reddy R, Patel SD, et al. 1997. T1ρ-relaxation in articular cartilage: Effects of enzymatic degradation. Magnetic resonance in medicine 38: 863-867.

18. Nieminen MT, Rieppo J, Töyräs J, et al. 2001. T2 relaxation reveals spatial collagen architecture in articular cartilage: A comparative quantitative MRI and polarized light microscopic study. Magnetic resonance in medicine 46: 487-493.

19. Chavhan GB, Babyn PS, Thomas B, Shroff MM, Haacke EM. 2009. Principles, techniques, and applications of T2*-based MR imaging and its special applications. Radiographics 29: 1433-1449.

20. Mamisch TC, Hughes T, Mosher TJ, et al. 2012. T2 star relaxation times for assessment of articular cartilage at 3 T: A feasibility study. Skeletal Radiol 41: 287-292.

21. Borthakur A, Mellon E, Niyogi S, et al. 2006. Sodium and T1ϱ MRI for molecular and diagnostic imaging of articular cartilage. NMR Biomed 19: 781-821.

22. Jones EF, Schooler J, Miller DC, et al. 2012. Characterization of human osteoarthritic cartilage using optical and magnetic resonance imaging. Molecular Imaging and Biology 14: 32-39.

23. Williams A, Gillis A, McKenzie C, et al. 2004. Glycosaminoglycan distribution in cartilage as determined by delayed gadolinium-enhanced MRI of cartilage (dGEMRIC): Potential clinical applications. Am J Roentgenol 182: 167-172.

24. Wheaton AJ, Borthakur A, Shapiro EM, et al. 2004. Proteoglycan loss in human knee cartilage: Quantitation with sodium MR Imaging—Feasibility Study1. Radiology 231: 900-905.

25. Insko EK, Kaufman JH, Leigh JS, Reddy R. 1999. Sodium NMR evaluation of articular cartilage degradation. Magnetic resonance in medicine 41: 30-34.

26. Van Dyck P, Kenis C, Vanhoenacker FM, et al. 2014. Comparison of 1.5-and 3-T MR imaging for evaluating the articular cartilage of the knee. Knee Surgery, Sports Traumatology, Arthroscopy 1-9.

27. Kijowski R, Blankenbaker DG, del Rio AM, Baer GS, Graf BK. 2013. Evaluation of the articular cartilage of the knee joint: Value of adding a T2 mapping sequence to a routine MR imaging protocol. Radiology 267: 503-513.

28. Schooler J, Kumar D, Nardo L, et al. 2013. Longitudinal evaluation of T1ϱ and T2 spatial distribution in osteoarthritic and healthy medial knee cartilage. Osteoarthritis and Cartilage .

29. Van Tiel J, Bron E, Tiderius C, et al. 2013. Reproducibility of 3D delayed gadolinium enhanced MRI of cartilage (dGEMRIC) of the knee at 3.0 T in patients with early stage osteoarthritis. Eur Radiol 23: 496-504.

30. Deniz CM, Brown R, Lattanzi R, et al. 2013. Maximum efficiency radiofrequency shimming: Theory and initial application for hip imaging at 7 tesla. Magn Reson Imaging 69: 1379-1388.

31. Chang G, Diamond M, Nevsky G, Regatte R, Weiss D. 2013. Early knee changes in dancers identified by ultra-high-field 7 T MRI. Scand J Med Sci Sports .

32. Chang G, Deniz CM, Honig S, et al. 2013. MRI of the hip at 7T: Feasibility of bone microarchitecture, high-resolution cartilage, and clinical imaging. Journal of Magnetic Resonance Imaging .

33. Juras V, Welsch G, Bär P, et al. 2012. Comparison of 3T and 7T MRI clinical sequences for ankle imaging. Eur J Radiol 81: 1846-1850.

34. Moon CH, Kim J, Zhao T, Bae KT. 2013. Quantitative 23Na MRI of human knee cartilage using dual-tuned 1H/23Na transceiver array radiofrequency coil at 7 tesla. Journal of Magnetic Resonance Imaging 38: 1063-1072.

35. Madelin G, Chang G, Otazo R, Jerschow A, Regatte RR. 2012. Compressed sensing sodium MRI of cartilage at 7T: Preliminary study. Journal of Magnetic Resonance 214: 360-365.

36. Vedrine P, Aubert G, Belorgey J, et al. 2014. Manufacturing of the Iseult/INUMAC whole body 11.7 T MRI magnet. Applied Superconductivity, IEEE Transactions on 24: 1-6.

37. Vedrine P, Abdel Maksoud W, Aubert G, et al. 2012. Latest progress on the Iseult/INUMAC whole body 11.7 T MRI magnet. Applied Superconductivity, IEEE Transactions on 22: 4400804-4400804.

38. van Nierop LE, Slottje P, van Zandvoort MJ, de Vocht F, Kromhout H. 2012. Effects of magnetic stray fields from a 7 tesla MRI scanner on neurocognition: A double-blind randomised crossover study. Occup Environ Med 69: 759-766.

39. Kido M, Ikoma K, Hara Y, et al. 2013. Selective visualization of rabbit knee cartilage using MR imaging with a double-contrast agent. Journal of Magnetic Resonance Imaging .

40. Apprich S, Mamisch T, Welsch G, et al. 2012. Quantitative T2 mapping of the patella at 3.0 T is sensitive to early cartilage degeneration, but also to loading of the knee. Eur J Radiol 81: e438-e443.

41. Zumstein V, Kraljević M, Conzen A, Hoechel S, Müller-Gerbl M. 2013. Thickness distribution of the glenohumeral joint cartilage: A quantitative study using computed tomography. Surgical and Radiologic Anatomy 1-5.

42. Hirvasniemi J, Kulmala K, Lammentausta E, et al. 2012. < i> in vivo</i> comparison of delayed gadolinium-enhanced MRI of cartilage and delayed quantitative CT arthrography in imaging of articular cartilage. Osteoarthritis and Cartilage .

43. Bansal P, Joshi N, Entezari V, Grinstaff M, Snyder B. 2010. Contrast enhanced computed tomography can predict the glycosaminoglycan content and biomechanical properties of articular cartilage. Osteoarthritis and cartilage 18: 184-191.

44. Bansal P, Stewart R, Entezari V, Snyder B, Grinstaff M. 2011. Contrast agent electrostatic attraction rather than repulsion to glycosaminoglycans affords a greater contrast uptake ratio and improved quantitative CT imaging in cartilage. Osteoarthritis and Cartilage 19: 970-976.

45. Silvast T, Jurvelin J, Aula A, Lammi M, Töyräs J. 2009. Contrast agent-enhanced computed tomography of articular cartilage: Association with tissue composition and properties. Acta Radiol 50: 78-85.

46. Kokkonen H, Jurvelin J, Tiitu V, Töyräs J. 2011. Detection of mechanical injury of articular cartilage using contrast enhanced computed tomography. Osteoarthritis and Cartilage 19: 295-301.

47. Silvast TS, Kokkonen HT, Jurvelin JS, et al. 2009. Diffusion and near-equilibrium

distribution of MRI and CT contrast agents in articular cartilage. Phys Med Biol 54: 6823.

48. Nagarajan M, Coan P, Huber M, et al. 2013. Computer-aided diagnosis in phase contrast X-ray computed tomography for quantitative characterization of ex vivo human patellar cartilage. IEEE Trans Biomed Eng 60: 2896-2903.

49. Batiste DL, Kirkley A, Laverty S, et al. 2004. Ex vivo characterization of articular cartilage and bone lesions in a rabbit ACL transection model of osteoarthritis using MRI and micro-CT1. Osteoarthritis and cartilage 12: 986-996.

50. Wang G, Zhao S, Yu H, et al. 2005. Design, analysis and simulation for development of the first clinical micro-CT scanner. Acad Radiol 12: 511-525.

51. Chu CR, Lin D, Geisler JL, et al. 2004. Arthroscopic microscopy of articular cartilage using optical coherence tomography. Am J Sports Med 32: 699-709.

52. Pan Y, Li Z, Xie T, Chu CR. 2003. Hand-held arthroscopic optical coherence tomography for in vivo high-resolution imaging of articular cartilage. J Biomed Opt 8: 648-654.

53. te Moller N, Brommer H, Liukkonen J, et al. 2013. Arthroscopic optical coherence tomography provides detailed information on articular cartilage lesions in horses. The Veterinary Journal 197: 589-595.

54. Li X, Martin S, Pitris C, et al. 2005. High-resolution optical coherence tomographic imaging of osteoarthritic cartilage during open knee surgery. Arthritis research & therapy 7: R318.

55. Chu CR, Williams A, Tolliver D, et al. 2010. Clinical optical coherence tomography of early articular cartilage degeneration in patients with degenerative meniscal tears. Arthritis & Rheumatism 62: 1412-1420.

56. Saarakkala S, Wang S, Huang Y, Zheng Y. 2009. Quantification of the optical surface reflection and surface roughness of articular cartilage using optical coherence tomography. Phys Med Biol 54: 6837.

57. Huang Y, Saarakkala S, Toyras J, et al. 2011. Effects of optical beam angle on quantitative optical coherence tomography (OCT) in normal and surface degenerated bovine articular cartilage. Phys Med Biol 56: 491.

58. Wang S, Huang Y, Wang Q, Zheng Y, He Y. 2010. Assessment of depth and degeneration dependences of articular cartilage refractive index using optical coherence tomography in vitro. Connect Tissue Res 51: 36-47.

59. Herrmann J, Pitris C, Bouma B, et al. 1999. High resolution imaging of normal and osteoarthritic cartilage with optical coherence tomography. J Rheumatol 26: 627-635.

60. Saarakkala S, Waris P, Waris V, et al. 2012. Diagnostic performance of knee ultrasonography for detecting degenerative changes of articular cartilage. Osteoarthritis and Cartilage 20: 376-381.

61. Lee C, Huang M, Chai C, et al. 2008. The validity of in vivo ultrasonographic grading of osteoarthritic femoral condylar cartilage: A comparison with in vitro ultrasonographic and histologic gradings. Osteoarthritis and Cartilage 16: 352-358.

62. Adler RS, Dedrick DK, Laing TJ, et al. 1992. Quantitative assessment of cartilage surface roughness in osteoarthritis using high frequency ultrasound. Ultrasound Med Biol 18: 51-58.

63. Saarakkala S, Töyräs J, Hirvonen J, et al. 2004. Ultrasonic quantitation of superficial degradation of articular cartilage. Ultrasound Med Biol 30: 783-792.

64. Liukkonen J, Hirvasniemi J, Joukainen A, et al. 2013. Arthroscopic ultrasound technique for simultaneous quantitative assessment of articular cartilage and subchondral bone: An< i> in Vitro</i> and< i> in Vivo</i> feasibility study. Ultrasound Med Biol .

65. Töyräs J, Rieppo J, Nieminen M, Helminen H, Jurvelin J. 1999. Characterization of enzymatically induced degradation of articular cartilage using high frequency ultrasound. Phys Med Biol 44: 2723.

66. Hattori K, Takakura Y, Ishimura M, et al. 2005. Differential acoustic properties of early cartilage lesions in living human knee and ankle joints. Arthritis & Rheumatism 52: 3125-3131.

67. Saied A, Cherin E, Gaucher H, et al. 1997. Assessment of articular cartilage and subchondral bone: Subtle and progressive changes in experimental osteoarthritis using 50 MHz echography in vitro. Journal of bone and mineral research 12: 1378-1386.

68. Kaleva E, Virén T, Saarakkala S, et al. 2011. Arthroscopic ultrasound assessment of articular cartilage in the human knee joint A potential diagnostic method. Cartilage 2: 246-253.

69. Wang Q, Zheng Y, Qin L, et al. 2008. Real-time ultrasonic assessment of progressive proteoglycan depletion in articular cartilage. Ultrasound Med Biol 34: 1085-1092.

70. Viren T, Saarakkala S, Tiitu V, et al. 2011. Ultrasound evaluation of mechanical injury of bovine knee articular cartilage under arthroscopic control. Ultrasonics, Ferroelectrics and Frequency Control, IEEE Transactions on 58: 148-155.

71. Legare A, Garon M, Guardo R, et al. 2002. Detection and analysis of cartilage degeneration by spatially resolved streaming potentials. Journal of orthopaedic research 20: 819-826.

72. Préville A, Lavigne P, Buschmann M, et al. 2013. Electroarthrography: A novel method to assess articular cartilage and diagnose osteoarthritis by non-invasive measurement of load-induced electrical potentials at the surface of the knee. Osteoarthritis and Cartilage 21: 1731-1737.

73. Morita Y, Kondo H, Tomita N, Suzuki S. 2012. A feasibility study for evaluation of mechanical properties of articular cartilage with a two-electrode electrical

impedance method. Journal of Orthopaedic Science 17: 272-280.

74. Frank EH, Grodzinsky AJ, Koob TJ, Eyre DR. 1987. Streaming potentials: A sensitive index of enzymatic degradation in articular cartilage. Journal of orthopaedic research 5: 497-508.

75. Changoor A, Coutu JP, Garon M, et al. 2011. Streaming potential-based arthroscopic device is sensitive to cartilage changes immediately post-impact in an equine cartilage injury model. J Biomech Eng 133: 278.

76. Abedian R, Willbold E, Becher C, Hurschler C. 2013. In vitro electro-mechanical characterization of human knee articular cartilage of different degeneration levels: A comparison with ICRS and mankin scores. J Biomech .

77. Novakofski KD, Williams RM, Fortier LA, et al. 2013. Identification of cartilage injury using quantitative multiphoton microscopy. Osteoarthritis and Cartilage .

78. Ross KA, Williams RM, Schnabel LV, et al. 2013. Comparison of three methods to quantify repair cartilage collagen orientation. Cartilage 4: 111-120.

79. Zipfel WR, Williams RM, Christie R, et al. 2003. Live tissue intrinsic emission microscopy using multiphoton-excited native fluorescence and second harmonic generation. Proc Natl Acad Sci U S A 100: 7075.

80. Centonze VE, White JG. 1998. Multiphoton excitation provides optical sections from deeper within scattering specimens than confocal imaging. Biophys J 75: 2015-2024.

81. Yeh AT, Hammer-Wilson MJ, Van Sickle DC, et al. 2005. Nonlinear optical microscopy of articular cartilage. Osteoarthr Cartilage 13: 345-352.

82. Brockbank KGM, MacLellan WR, Xie J, et al. 2008. Quantitative second harmonic generation imaging of cartilage damage. Cell Tissue Banking 9: 299-307.

83. Mansfield J, Yu J, Attenburrow D, et al. 2009. The elastin network: Its relationship with collagen and cells in articular cartilage as visualized by multiphoton microscopy. J Anat 215: 682-691.

84. Williams RM, Zipfel WR, Tinsley ML, Farnum CE. 2007. Solute transport in growth plate cartilage: In vitro and in vivo. Biophys J 93: 1039-1050.

85. Da Costa V, Wei R, Lim R, et al. 2008. Nondestructive imaging of live human keloid and facial tissue using multiphoton microscopy. Archives of Facial Plastic Surgery 10: 38.

86. Pavlova I, Hume KR, Yazinski SA, et al. 2010. Multiphoton microscopy as a diagnostic imaging modality for lung cancer. Proc Soc Photo Opt Instrum Eng 7569: 756918.

87. Wang CC, Li FC, Wu RJ, et al. 2009. Differentiation of normal and cancerous lung tissues by multiphoton imaging. J Biomed Opt 14: 044034.

88. Skala MC, Squirrell JM, Vrotsos KM, et al. 2005. Multiphoton microscopy of endogenous fluorescence differentiates normal, precancerous, and cancerous squamous epithelial tissues. Cancer Res 65: 1180.

CHAPTER 2

IDENTIFICATION OF CARTILAGE INJURY USING QUANTITATIVE MULTIPHOTON MICROSCOPY

[1]Kira D. Novakofski, M.S., [2]Rebecca M. Williams, Ph.D., [1]Lisa A. Fortier, Ph.D., D.V.M., [3]Hussni O. Mohammed, Ph.D., [2]Warren R. Zipfel, Ph.D., [2]Lawrence J. Bonassar, Ph.D.

[1]Department of Clinical Sciences, Cornell University, Ithaca, New York; [2]Department of Biomedical Engineering, [3]Population Medicine and Diagnostic Sciences, Cornell University, Ithaca, New York 14853, Cornell University, Ithaca, New York 14853

Published in Osteoarthritis and Cartilage [published online ahead of print November 1, 2013] doi:10.1016/j.joca.2013.10.008

ABSTRACT

Objective. Cartilage injury can lead to post-traumatic osteoarthritis (PTOA). Immediate post-trauma cellular and structural changes are not widely understood. Furthermore, current cellular-resolution cartilage imaging techniques require sectioning of cartilage and/or use of dyes not suitable for patient imaging. In this study, we used multiphoton microscopy (MPM) data with FDA-approved sodium fluorescein to identify and evaluate the pattern of chondrocyte death after traumatic injury.

Method. Mature equine distal metacarpal or metatarsal osteochondral blocks (OCBs) were injured by 30 MPa compressive loading delivered over 1 s. Injured and control sites were imaged unfixed and *in situ* 1 h post-injury with sodium fluorescein using rasterized z-scanning. MPM data was quantified in MATLAB, reconstructed in 3-D, and projected in 2-D to determine the damage pattern.

Results. MPM images (600 per sample) were reconstructed and analyzed for cell death. The overall distribution of cell death appeared to cluster into circular (n=7) or elliptical (n=4) patterns ($p=0.006$). Dead cells were also prevalent near cracks in the matrix, with only 26.3% (SE=5.0%, $p<0.0001$) of chondrocytes near cracks being viable.

Conclusion. This study demonstrates the first application of MPM for evaluating cellular-scale cartilage injury *in situ* in live tissue, with clinical potential for detecting early cartilage damage. With this technique, we were able to uniquely observe two death patterns resulting from the same compressive loading, which may be related to local variability in matrix structure. These results demonstrate proof-of-concept MPM diagnostic use in detecting subtle and early cartilage damage not detectable in any other way.

INTRODUCTION

Osteoarthritis (OA) is a degenerative, multifactorial disease affecting the world population.[1-3] Knowledge of severe cartilage damage has led to therapies targeting symptom management, but understanding the early events in OA can facilitate the development of effective modalities in disease intervention. However, limited high resolution imaging of cartilage damage in the clinical setting has hindered early disease identification. Current medical imaging modalities including magnetic resonance imaging (MRI) and computed tomography (CT) do not have the resolution necessary to detect small cartilage injuries that can occur after joint trauma which lead to post-traumatic osteoarthritis (PTOA). Without the ability to detect these micron-sized structural or cellular changes, it is difficult to understand the progression of PTOA and facilitate its prevention. Developing methods for detecting early cartilage damage *in vivo* can expand the understanding of cartilage degeneration immediately after tissue damage.

Multiphoton microscopy (MPM) is capable of imaging live biological samples, including cartilage at submicron resolution, yielding structural details at depths greater than possible with confocal microscopy.[4] Importantly, MPM can be adapted for *in vivo* imaging with diagnostic application, including distinguishing normal vs abnormal or cancerous tissue,[5-8] and it is being developed into a fast-scanning endoscope.[9] Diagnostic *in vivo* MPM can be adapted to cartilage because of the high collagen content of the cartilage extracellular matrix (ECM). Collagen emits second harmonic generation (SHG), making it readily detectable without staining.[10] Collecting SHG signal allows the general collagen matrix of the cartilage to be easily observed. Additionally, many molecules autofluoresce with MPM,[4] and additional dyes may be used to further characterize tissue. Although fluorescent techniques have greatly expanded our understanding of cell biology, fluorescent labeling typically uses dyes

that are unsuitable for clinical use. Sodium fluorescein is FDA-approved and is used ophthalmologically or intravenously to diagnose blood vessel disorders and corneal abrasions. Sodium fluorescein has been shown to stain cells[11] by binding non-specifically to proteins,[12] making it an attractive method to label cells that have compromised membranes and may be dead. Imaging in a highly fluorescent solution like fluorescein can be difficult, but the optical capabilities of MPM make it possible. SHG and fluorescein can be used to collect high resolution information from live tissue to study the mechanisms involved in the progression of cartilage damage.

The importance of understanding the early sequence of events between cartilage trauma and OA is at the forefront of arthritis research.[2,13-15] Cell death has been shown to occur after traumatic injury,[2,15] but the immediate effect of compressive trauma on chondrocyte viability[15] and the resulting dispersion of cell death and matrix damage around the injury site have not been studied in detail. The spatial distribution of chondrocyte death may be influenced by many factors. The superficial zone has been shown to be more susceptible than deeper cartilage layers to compressive injury.[16] This phenomenon may result from zonal ECM composition and collagen orientation, which distribute load when force is applied.[17,18] Evaluating chondrocyte death distrubtion in the superficial zone with MPM can further elucidate these underlying structural factors.

The goal of the current study was to use MPM to evaluate cellular damage after cartilage injury *ex vivo* in live tissue using an FDA-approved dye to detect chondrocyte death. Specifically, by using MPM with sodium fluorescein, we evaluated the pattern of chondrocyte death in the superficial zone immediately following traumatic injury like that which could contribute to the development of early PTOA.

METHODS

Tissue collection and injury model

The distal third metacarpus (n=3) or metatarsus (n=8) was harvested from the left (n=5) or right (n=6) limb of young adult horses (n=10, ages 4-6 years) immediately after being euthanized for reasons unrelated to this study under the guidelines and approval of the Institutional Animal Care and Use Committee. The limb was chosen at random. Cartilage was grossly evaluated and scored using the International Cartilage Repair Society (ICRS) Cartilage Injury Evaluation System (www.cartilage.org). Only healthy samples (i.e., those receiving scores of 0, 1a, or 1b) were used for the study. Osteochondral blocks (OCBs) were initially placed in HBSS with 100 IU/ml penicillin and 100 μg/ml streptomycin and then transferred to phenol red-free MEM containing 25 mM Hepes, 100 I.U./ml penicillin, and 100 μg/ml streptomycin. Dye-free media was used to prevent staining prior to microscopic imaging. In order to model early cartilage injury, OCBs were then briefly removed from the media and mounted between a custom-designed specimen-chamber and a 2.25 mm-diameter indenter on an EnduraTEC ELF3200 mechanical test frame (EnduraTec, Minnetonka, MN). The articular surface of the medial condyle, medial to the sagittal ridge and anterior to the transverse ridge, was injured under load-control with a single compression of 30 MPa[19] within 1 s (Fig. 2.1) (mean peak stress rate 118.5 MPa s^{-1} [95% confidence interval (CI) 115.7-121.3]; mean strain 63% [95% CI 52-74]; mean peak strain rate 587% s^{-1} [95% CI 310-864]). The lateral condyle functioned as the control. After injury, OCBs were placed back into the media and incubated for 1 h at 37°C in 5% CO_2.

MPM data acquisition and staining

After incubation, OCBs were placed in 1 μM sodium fluorescein (AK-FLOUR 25%,

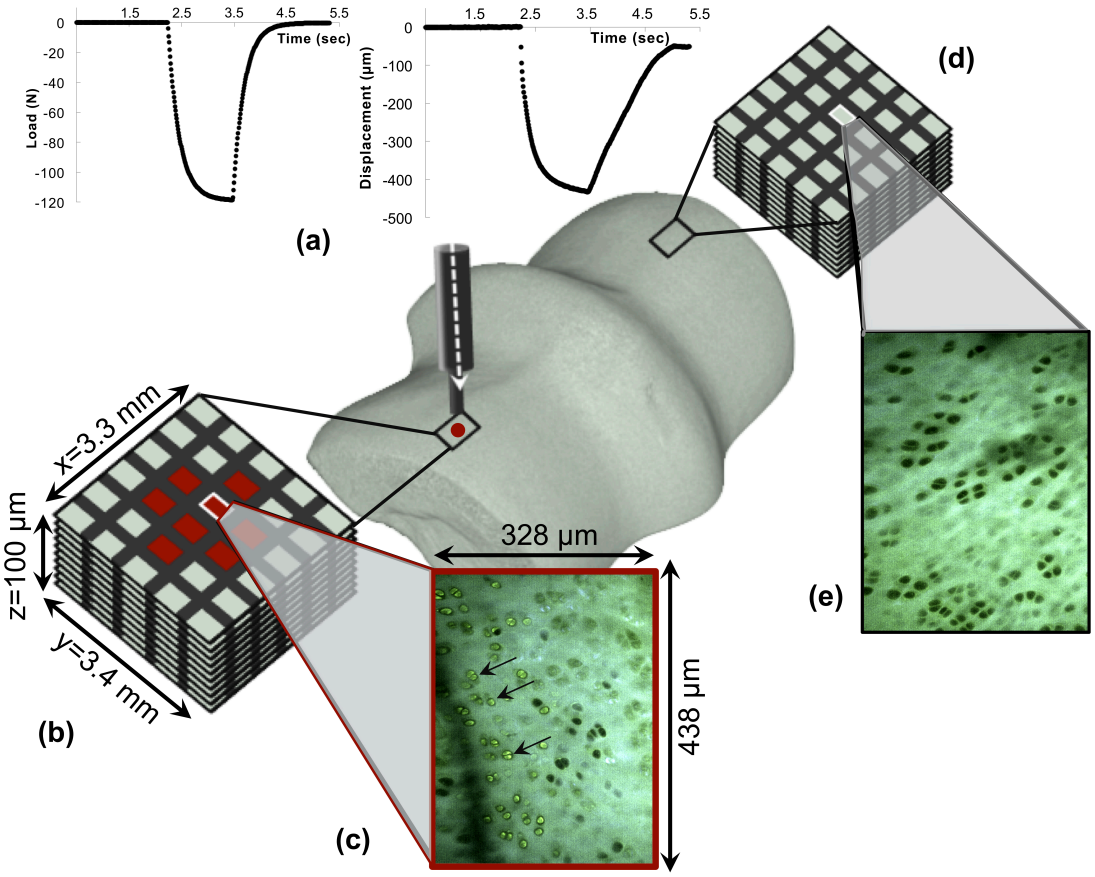

Figure 2.1. Schematic of methods. (**a**) An osteochondral block is injured with compressive loading. The injured site (**b**) and corresponding control site (**c**) are each scanned with multiphoton microscopy using a rasterized pattern, alternating scanned and non-scanned regions to encompass a 3.3 mm x 3.4 mm area. Individual 328 µm x 438 µm images that comprise the larger rasterized scanned area are shown in (**d**) and (**e**), with arrows denoting fluorescein-labeled dead cells.

Akorn, Inc., Lake Forest, IL) in PBS. Fluorescein was chosen for this study because it is FDA-approved and has been previously used for determining tissue viability *in vivo* in both animals and humans.[20,21] The ability of fluorescein to detect cell death was initially validated by dual staining of cartilage with 1 μM ethidium homodimer-1 (EthD-1, Invitrogen, Grand Island, NY) and fluorescein. Imaging was performed using a lab-built MPM instrument, in which an uncompensated beam from a modelocked Ti:sapphire laser (Tsunami pumped with a Millennia Xs; Newport, Irvine, CA) was passed through an Electro-Optic Modulator (350-80LA; Conoptics, Danbury, CT) with laboratory-built electronics for beam modulation and blanking during scan fly-back. The beam was then directed into a modified BioRad scanner (MRC-600) interfaced with a modified Olympus AX-70 upright microscope (Center Valley, PA). An excitation wavelength of 780 nm was delivered through an Olympus XLUMPlanFl 20X/0.95NA water immersion objective to obtain MPM images.[22] The emission signal was separated from the excitation beam using a 670 nm long-pass dichroic. Samples were placed in fluorescein solution for 10-15 min and then imaged within the solution. Data was collected first with fluorescein excited at 780 nm and collected through a 380-540 emission filter. EthD-1 was then added and allowed to incubate for 30 min, after which the imaging was repeated with the added EthD-1 signal collected through a 560-650 nm emission filter in a second detection channel. Using this approach fluorescein was validated as an indicator of cell death, and dual staining with EthD-1 was discontinued (n=9 sites, n=1 OCB). The remainder of the data was collected using only fluorescein.

After injury, OCBs were positioned on the MPM stage, maintaining medial-lateral orientation. The sample was imaged in the transverse plane with the same instrumentation as described above. Imaging was performed starting at the articular surface and penetrating 100 μm deep to encompass the superficial zone.[23] Cartilage

SHG and autofluorescence, and fluorescein fluorescence were collected by photomultiplier tubes using a 360-490 nm filter for autofluorescence and SHG from the cartilage matrix, and a 510-650 nm filter for fluorescein emission. Each z-stack acquired emission from 328 x 438 μm section, with ten 10 μm z-steps. A rasterized tile scan with x=272 μm and y=312 μm sized steps acquired data from a large field 4.528 x 4.938 mm area or small field 3.328 x 3.438 mm area of the injured region and surrounding tissue, and a respective scan of the control lateral condyle (Fig. 2.1, n=11 OCBs). Z-stacks were collected starting at the cartilage articular surface. The tiling algorithm detected the articular surface based on the emission signal intensity. The z-depth of the surface was recorded for subsequent 3D reconstruction. To minimize potential variation between samples resulting from the length of a high resolution tile scan, tiled images were collected in a grid with a reduced fill factor, resulting in 37% of the tissue being scanned. This fill factor was chosen in order to complete the small field scan within an hour. The small field scan was more readily utilized due to its shorter scan time. The large field was used on limited samples in order to confirm that the small field scan encompassed all dead chondrocytes.

After the rasterized tile scan was completed, along with additional samples, cartilage was removed from the bone to image in the sagittal plane (control n=13 OCBs from n=6 horses; injured n=10 OCBs from n=6 horses). This was performed to evaluate chondrocyte death at a depth greater than could be obtained by MPM imaging from the articular surface. Images were collected from a single z-depth penetration into the cross-section.

Chondrocyte death identification with MPM data analysis

Two-filter channel emission resulting from the transversely oriented, rasterized tile scan was processed in custom code created in MATLAB (MathWorks, Natick, MA).

All chondrocytes were identified in the 380-490 nm channel emission data using code similar to public MATLAB-published "Identifying Round Objects." The MPM emission grayscale image was first thresholded to a binary black and white image (graythresh, im2bw). Objects in the binary image were smoothed (bwareaopen), and any holes were filled (imfill) to create solid objects. The boundaries of these solid objects were identified (bwboundaries). The properties for each object including boundary coordinates, centroid coordinates, area, and perimeter were recorded (regionprops). If the area and perimeter were each above given threshold values, both of which were optimized for each horse, the object and its centroid were recorded as a chondrocyte. To accommodate for clonal cells, which were difficult for the image analysis program to separate, threshold parameters were optimized for single, double, and triple clustered cells by allowing small, medium, and large sized objects that were then counted as one, two, or three cells, respectively. Threshold parameters were adjusted for each animal set due to the variation in image intensity, cell size, and cell clustering between animals. Injured and control images within one animal were analyzed using the same parameters.

Dead chondrocytes were identified in the 510-650 nm channel. All object boundaries recorded from the code described above were evaluated in this channel. Each boundary was defined as the region-of-interest (roipoly), so that the presence or absence of fluorescein at this site could be determined. The mean intensity of the fluorescein image was first calculated; fluorescein-cells had an intensity above this mean, and an intensity threshold was optimized for each horse. If the bounded region was above this threshold, the cell(s) were recorded as dead.

Death pattern processing

The degree of circularity or ellipticity of the cell death pattern was determined for

each horse using MATLAB custom code that calculated eigenvectors and eigenvalues of two-dimensional projections of dead cell distributions obtained from tile scans. The covariance (cov) and central point (mean) of all dead cell centroid coordinates were calculated. The eigenvector and eigenvalues (eig) were calculated for the resulting covariance. The percent-difference between eigenvalues, or more simply the long- and short-axes, was then used to determine if the pattern of cell death was circular or elliptical, using a threshold of less than or greater than 30% percent-difference, respectively, between the long and short axes.

Cell death near cracks and as a function of depth

Z-stack images of the injured sites were examined to identify those that contained cracks within the ECM, which were similar to but not including the image shown in Fig. 2.2. Within these identified images, the z-stack image corresponding to 10 μm in depth from the surface was used for analysis, due to the clarity of the matrix. Within these images, each of the first three cells occurring within 100 μm distance from each crack was counted around the entire crack perimeter to determine cell death. Cracks were not observed in control samples.

Images from two-filter channel emission data from sagittal plane scans of full-thickness cartilage explants were manually stitched together. Then, all cells were manually counted at 50 μm steps, with fluorescein stained (dead) cells being recorded to calculate death as a function of depth.

Statistical analysis

The calculated percent difference between the eigenvectors of the circular and elliptical death patterns were clustered into their respective groupings and compared using a Wilcoxon rank sum test. A non-parametric test was used because the

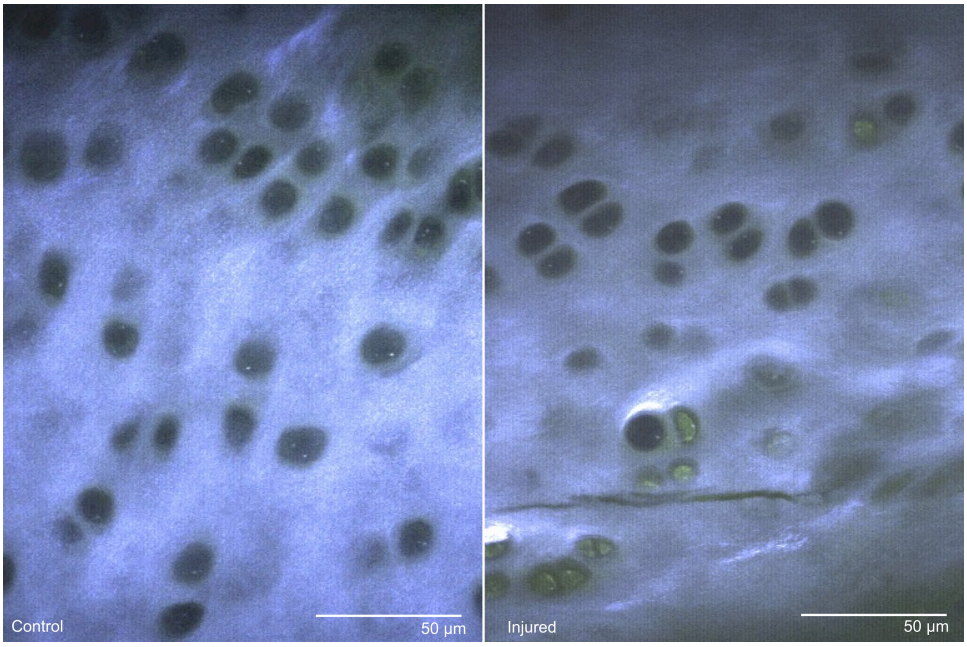

Figure 2.2. Multiphoton microscopy images from a single-image plane within a z-stack, from both control and injured samples. Signal from the 380-490 nm channel (blue) and 510-650 nm channel (green) have been merged for clarity, resulting in collagen SHG and ECM autofluorescence appearing blue-green and fluorescein-stained cells appearing green. Control samples typically contained few fluorescein-stained cells and had regular SHG signal within the ECM. Injured samples typically contained more fluorescein-stained cells and irregular SHG signal, resulting from damaged matrix, such as cracks.

difference was not normally distributed. Medians with ranges are reported. The percentage of chondrocyte death in the sagittal plane was evaluated at each 50 μm region using a two sample t-test, comparing control and injured samples. The same test was performed to compare chondrocyte death near cracks to controls. Statistical analyses were computed using Statistix 10.0 (Analytical Software, Tallahassee, FL) with $p<0.05$ considered significant.

RESULTS

Chondrocyte death identification from MPM data acquisition

MPM images provided high resolution detail of chondrocytes and the surrounding ECM. Each image collected was 328.7 x 438.3 μm in size. In separate studies, fluorescein was used with EthD-1 to verify that fluorescein can be used as an indicator of cell death. Cells were manually counted (n=9 sites, n=1 OCB), and fluorescein-staining correlated to EthD-1-staining with a linear relationship of slope 1.049 and squared correlation coefficient $r^2=0.929$ (Fig. 2.3).

Matrix-associated SHG signal allows for identification of chondrocyte lacunae as holes in the matrix. Control cartilage contained few chondrocytes with fluorescein staining. Images from the damaged regions contained more fluorescein-stained chondrocytes, autofluorescence, and irregular SHG signal, particularly near cracks (Figure 2). After injury, chondrocyte death was found to be significantly increased in the superficial 100 μm (Fig. 2.4, $p<0.05$).

Chondrocyte death spatial dispersion

The superficial 100 μm was evaluated in a medial-lateral ("x") and anterior-posterior axis ("y") coordinate system to understand the dispersion of cartilage death after traumatic injury in intact samples. A total of 420 control and 420 injured images for

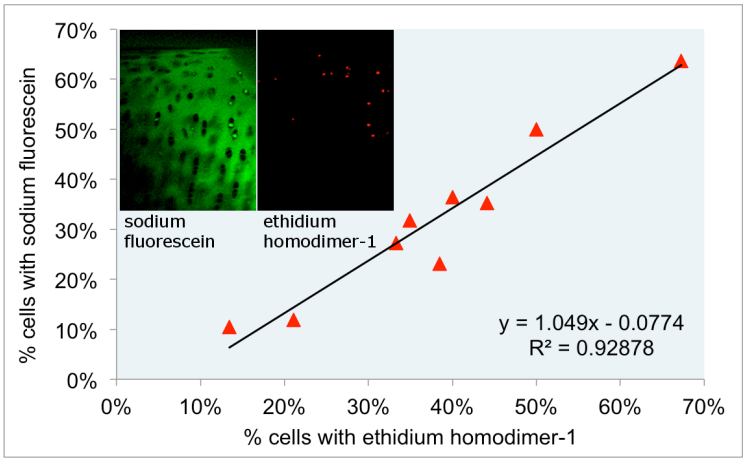

Figure 2.3. Sodium fluorescein and ethidium homodimer-1 validation. Cartilage was stained with both sodium fluorescein and ethidium homodimer-1 to determine the linear relationship between dyes to validate sodium fluorescein as a dead cell indicator. The linear relationship with a slope 1.049 and squared correlation coefficient r^2=0.929 was determined.

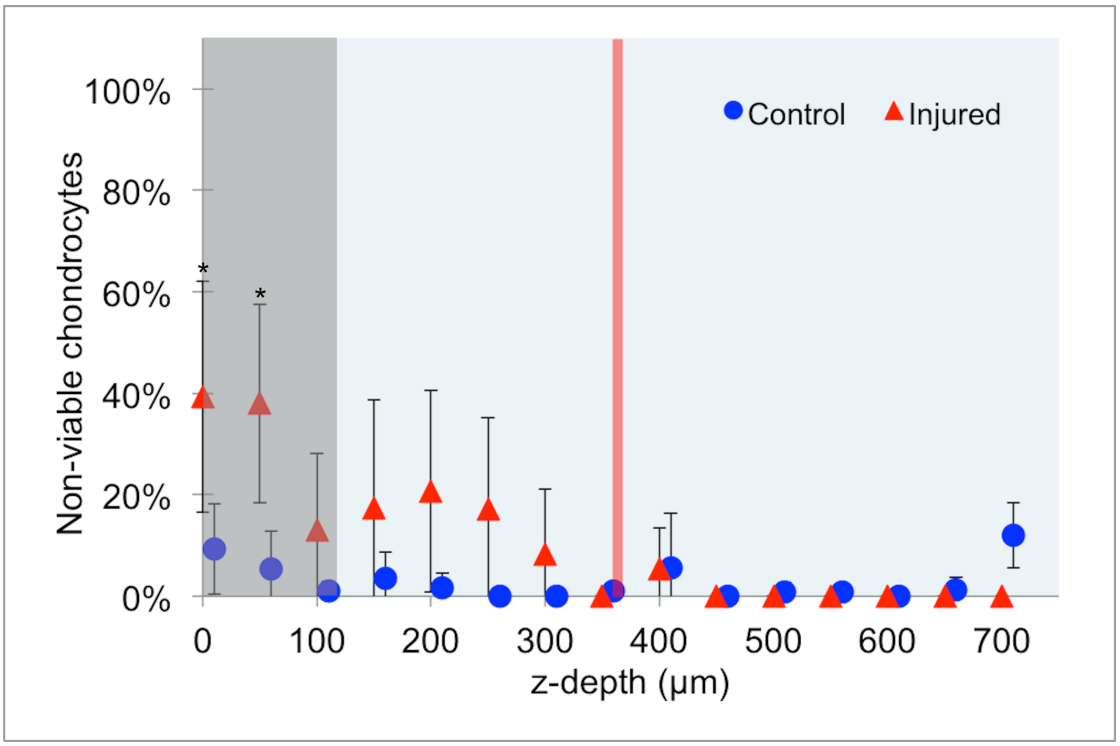

Figure 2.4. Percentage of dead chondrocytes after injury, as a function of depth in 50 μm steps, as measured in the sagittal plane. The box represents the depth to which transverse MPM images were acquired for rasterized tile scanning, as described in the methods. The line demonstrates the mean depth to which samples were compressed. A total of n=13 OCBs from n=6 horses were analyzed for controls; a total of n=10 OCBs from n=6 horses were injured. Data is represented as the mean ± 95% confidence intervals. * represents a significant difference between control and injured ($p<0.05$) using a two-sample t-test.

each sample were collected in the large field, and 300 control and 300 injured images for each sample in the small field. Centroids of dead cells were plotted in 3-D (Fig. 2.5) and projected into 2-D (Fig. 2.6) to determine the spatial pattern of damage. Dead cells were more numerous at the periphery of injury. The injury pattern was circular in some samples (n=7) and more elliptical (n=4) in others. Samples in which the percent-difference between the two eigenvalues was less than 30% of the minor eigenvalue were considered to have a circular damage pattern (17.7%, range 5.6-23.8%), while those in which this percent-difference was greater than 30% were considered to have an elliptical damage pattern (59.6%, range 39.0-162.9%). These values were statistically different from each other (p=0.006). The median peak load and peak displacement did not vary between groups with circular and elliptical damage patterns (Table 2.1).

Images were selected to evaluate local chondrocyte death within 100 μm of cracks, as identified by the absence of SHG signal (Figure 2). Cell death within 100 μm of cracks was significantly increased, with 73.7% (95% CI 64.0-83.4%, n=13 images from n=5 OCBs, $p<0.0001$) of cells being dead, compared to the corresponding control site images with cell death of 1.0% (95% CI 0-2.2%, n=13 images from n=5 OCBs).

DISCUSSION

This study used high resolution MPM imaging to determine the spatial distribution of chondrocyte death using a cartilage injury model. We demonstrated the feasibility of using MPM in live tissue, including collecting SHG signal and fluorescein emission, to detect subtle structural and cellular damage below the resolution of current clinical imaging techniques. With this technique, we were also able to identify two distributions of cell death that resulted from the same applied stress.

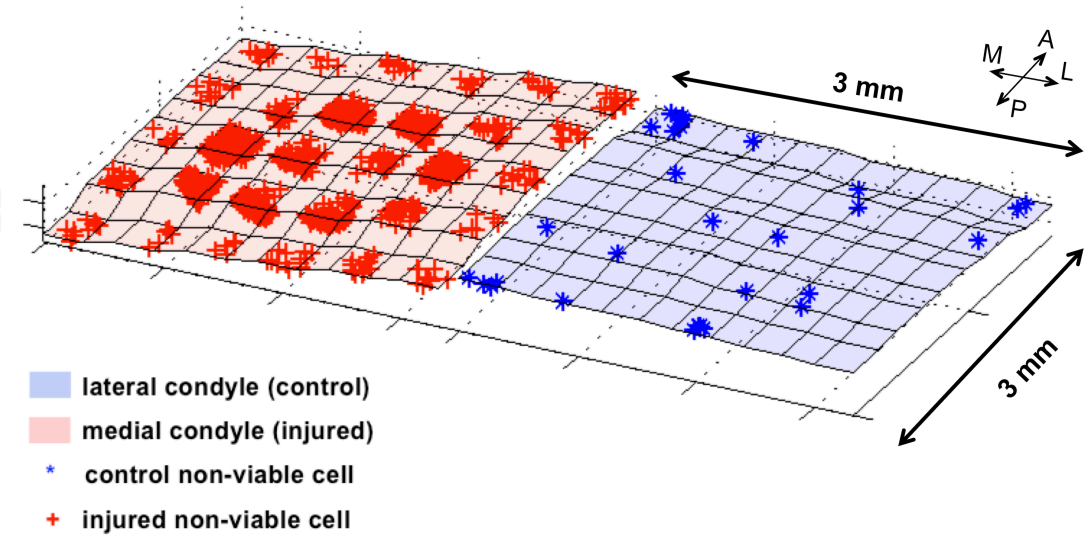

Figure 2.5. 3-D reconstructions of control and injured cartilage. Each blue point represents a single dead chondrocyte in the control scanned site; each red point represents a single dead chondrocyte in the injured scanned site.

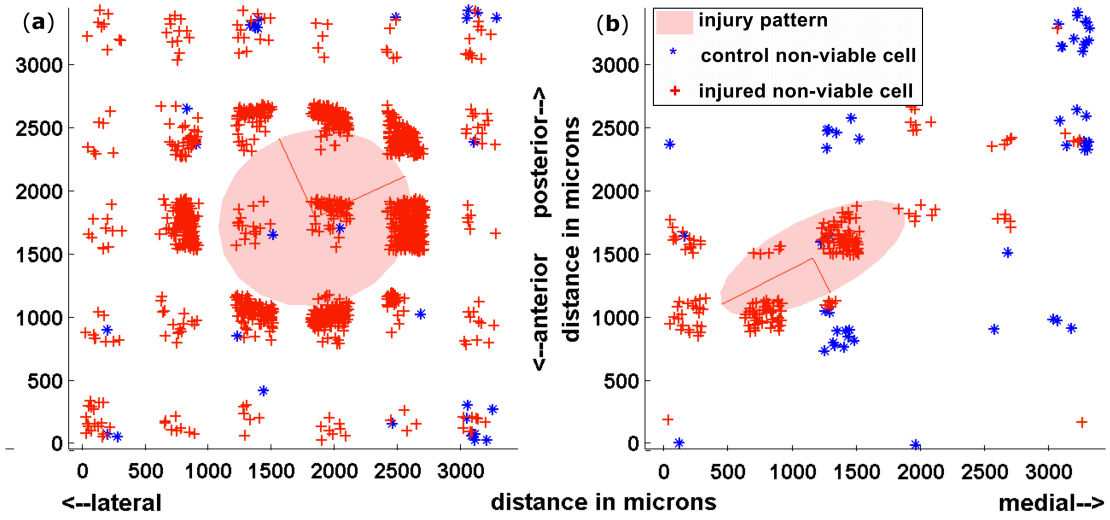

Figure 2.6. 2-D projections of control and injured cartilage. (**a**) A representative circular injury; (**b**) a representative elliptical injury. Each blue point represents a single dead chondrocyte in the control scanned site; each red point represents a single dead chondrocyte in the injured scanned site; the red lines represent the eigenvalues and eigenvectors; the transparent red shaded area denotes the area which corresponds with the eigenvectors.

	Load (N)	Displacement (μm)	Axes Difference (%)
Circular	117.74 (117.60-117.75)	319 (226-605)	17.7 (5.6-23.8)
Elliptical	117.69 (117.67-117.74)	373 (319-425)	59.6 (39.0-162.9)

Table 2.1. Median peak load (with range), median peak displacement (with range), and median percent-difference between the long- and short-axis (with range). The difference of 30% was used to classify groups into "circular" (n=7) and "elliptical" (n=4) damage patterns.

SHG and fluorescein were used to detect structural damage and cell death as shown in Figure 2. Chondrocyte lacunae can be easily identified, even in non-stained cartilage tissue, due to the absence of SHG signal within the lacunae. In other imaging techniques where the ECM is not easily identified, multiple dyes must be added to identify the matrix and live or dead cells, but these dyes cannot be used clinically. In this study, fluorescein was shown to strongly correlate with EthD-1. Because sodium fluorescein is FDA-approved and can detect damaged cells, it shows promise as a diagnostic method for *in vivo* microscopic imaging of damaged cartilage. Overall, we were able to use one dye with MPM imaging to quantify early damage following cartilage injury in live cartilage.

Matrix damage was also identified using MPM due to the irregularities in SHG. Using SHG, cracks as narrow as 2 μm were identified and associated with significant increase in chondrocyte death. This finding is similar to previous work examining chondrocyte death near large cracks and fissures 18 h after injury.[24] Although we did not quantify SHG emission, work by Brockbank *et al* showed that thermally-damaged cartilage has decreased SHG,[25] suggesting that SHG may be an additional measurement for damaged matrix, likely due to decreased collagen organization. Collagen organization was not determined because type II fibrils are generally sub-resolution in all types of optical microscopy. Overall, we were able to observe maximal information about the cellular and structural qualities of cartilage, while using a minimally invasive technique and labeling strategy.

MPM has been used as a diagnostic tool in other fields,[5,8,9] and this study demonstrated the feasibility of applying MPM and fluorescein to arthroscopic evaluation of cartilage *in vivo*. Endoscopic MPM has been demonstrated,[9] providing feasibility for MPM as an arthroscopic tool. Fluorescein could be readily added to fluids used routinely during arthroscopy. Other techniques for detecting cartilage

injury in live tissue, such as the work by Changoor *et al*. in examining electromechanical properties, are valuable but do not measure biological or cellular changes.[26] Optical coherence tomography (OCT) and ultrasound imaging (UI) have also been used for high resolution evaluation of live cartilage. OCT resolution is approximately 10-30 μm,[27-29] and UI is about 30-65 μm.[30] While their x-y-resolution is not as high as MPM, OCT and UI have z-depth capabilities of 1.10 mm[31] and 1.65 mm,[32] respectively. These techniques, however, only offer structural information. If UI is hybridized with fluorescence decay spectroscopy, biochemical information can also be ascertained,[30] albeit without the imaging resolution of MPM. Overall, the present study demonstrated the unique high resolution capabilities of MPM to detect cartilage damage in intact, live samples with the expectation of adaptation for *in vivo* arthroscopy.

Using MPM, we were able to identify the distribution of chondrocyte death after injury. We utilized 30 MPa which, based on previous ground force reaction studies in the equine forelimb, is about two- to three-fold physiologic loading.[33] These higher stresses have been shown to cause increased cell death[19] and was similarly found to cause an increase in cell death in this study. Many biochemical and biomechanical changes occur following traumatic injuries,[2,34] including decreased chondrocyte viability and increased catabolic gene expression.[14-16,35] While these studies suggest that key changes such as gene expression occur immediately after injury, the immediate consequences of a single traumatic load on cell death distribution are not known and were therefore examined in the present study. OCBs were injured to evaluate death distribution as a model of rapid change after cartilage injury. Samples were compressed, based on previous work,[19] with a loading rate similar to that which has been shown to result in surface fissures and large distribution of cell death in bovine metcarpal cartilage, 4 days after injury.[35] In this latter study,

Ewers *et al* stated that their unpublished preliminary data suggested that the majority of cell death occurred within 3 h following injury.[35] We specifically focused on cell death within this first hour to evaluate the immediate effects of mechanical injury and not of later apoptosis. MPM images of the most superficial 100 μm were collected. While other studies have removed the superficial layer prior to compression,[36] Chen *et al* found that bovine cartilage subjected to sustained continuous or cyclical loading up to 5 MPa primarily has decreased viability in the most superficial 70 μm.[16] After MPM acquisition, all lacunae were identified within the images, with the location of each dead chondrocyte being reconstructed and mapped. Overall, we found numerous dead chondrocytes at the periphery of the injured site, with fewer dead cells at the center of the injured site. This was not surprising because tissue under the center of the flat-ended indenter experiences high compressive strain and hydrostatic pressure, while the tissue at the edges of the indenter experiences high shear strains. Based on previous studies estimating shear stresses that produce cracks in cartilage in impact loading and finite element studies of local shear stresses during indentation, local shear stresses at the indenter edge were estimated to be 3.3-5.4 MPa.[27,37,38] As in previous studies,[39,40] cell death appears to be more prevalent in regions of tissue that experience high shear strain. Both with respect to x-y location, where cell death occurred preferentially near the edge of the indenter, and with respect to z-depth, where cell death occurred in regions within 200-400 μm from the surface, is the region known to experience highest shear strains. The dead-chondrocyte maps in the x-y plane were then analyzed using eigenvector analysis, and subsequently the axes of the spatial pattern to be calculated. This method was effective at revealing the patterns of cell death.

The observed injured samples were grouped into either circular (n=7) or elliptical (n=4) distribution patterns of chondrocyte death. All elliptical patterns were

found in metatarsus samples; however, due to the small metacarpus sample size, statistical analysis between the hind and forelimbs was not performed. These different precipitating patterns of cell death have not been previously described. Although care was taken to injure the same location in each specimen, there could have been slight variability in injury location due to the necessity of applying the load to the sample surface perpendicularly, and, therefore, also variability in cartilage matrix organization including orientation of collagen. Ugryumova *et al* has shown that the transverse orientation of collage in the superficial zone has a distinct pattern but varies highly by location.[18] This suggests that in the present study, differences in collagen orientation between injured sites within a sample may have occurred even if the injury sites were within millimeters of each other. To minimize this variation in collagen orientation, the medial condyle was consistently used as the injury site. While samples were not imaged prior to injury, the immediate surrounding regions near the injury site had a similar death staining pattern as the controls. Although only samples with an ICRS gross score of 0 or 1 were used, the background of the horses was unknown, which may introduce inter-animal variability. Collectively, these results suggest that the physiological consequences of trauma to the articular surface are site-dependent, which is important for understanding progression of PTOA between anatomic sites in patients.[14,15]

In summary, this study demonstrates the successful use of MPM imaging to detect cartilage damage in live tissue just one hour after injury. Cellular and structural changes that are below the resolution of other imaging techniques were readily identified with the fluorescein and MPM. Two unique injury patterns were observed suggesting that the cellular and structural consequences of injury are site-dependent or biologically variable. These findings may be significant for understanding, diagnosing and preventing PTOA development after injury. This study demonstrated the

feasibility of high resolution MPM imaging of live, intact cartilage for application *in vivo* to further the understanding about the early pathogenesis of cartilage injury that may lead to PTOA.

REFERENCES

1. Woolf AD, Pfleger B. 2003. Burden of major musculoskeletal conditions. Bull World Health Organ 81: 646-656.

2. Natoli RM, Scott CC, Athanasiou KA. 2008. Temporal effects of impact on articular cartilage cell death, gene expression, matrix biochemistry, and biomechanics. Ann Biomed Eng 36: 780-792.

3. Borrelli Jr J, Silva MJ, Zaegel MA, Franz C, Sandell LJ. 2009. Single high-energy impact load causes posttraumatic OA in young rabbits via a decrease in cellular metabolism. J Ortho Res 27: 347-352.

4. Zipfel WR, Williams RM, Christie R, et al. 2003. Live tissue intrinsic emission microscopy using multiphoton-excited native fluorescence and second harmonic generation. Proc Natl Acad Sci U S A 100: 7075.

5. Da Costa V, Wei R, Lim R, et al. 2008. Nondestructive imaging of live human keloid and facial tissue using multiphoton microscopy. Archives of Facial Plastic Surgery 10: 38.

6. Pavlova I, Hume KR, Yazinski SA, et al. 2010. Multiphoton microscopy as a diagnostic imaging modality for lung cancer. Proc Soc Photo Opt Instrum Eng 7569: 756918.

7. Wang CC, Li FC, Wu RJ, et al. 2009. Differentiation of normal and cancerous lung tissues by multiphoton imaging. J Biomed Opt 14: 044034.

8. Skala MC, Squirrell JM, Vrotsos KM, et al. 2005. Multiphoton microscopy of endogenous fluorescence differentiates normal, precancerous, and cancerous squamous epithelial tissues. Cancer Res 65: 1180.

9. Rivera DR, Brown CM, Ouzounov DG, et al. 2011. Compact and flexible raster scanning multiphoton endoscope capable of imaging unstained tissue. P Natl Acad Sci USA 108: 17598-17603.

10. Yeh AT, Hammer-Wilson MJ, Van Sickle DC, et al. 2005. Nonlinear optical microscopy of articular cartilage. Osteoarthr Cartilage 13: 345-352.

11. Mokhtarzadeh M, Casey R, Glasgow BJ. 2011. Fluorescein punctate staining traced to superficial corneal epithelial cells by impression cytology and confocal microscopy. Invest Ophthalmol Vis Sci 52: 2127-2135.

12. Andersson LO, Rehnström A, Eaker DL. 1971. Studies on "Nonspecific" binding. Eur J Biochem 20: 371-380.

13. Anderson DD, Chubinskaya S, Guilak F, et al. 2011. Post-traumatic osteoarthritis: Improved understanding and opportunities for early intervention. J Orthop Res 29: 802-809.

14. Backus JD, Furman BD, Swimmer T, et al. 2011. Cartilage viability and catabolism in the intact porcine knee following transarticular impact loading with and without articular fracture. J Orthop Res 29: 501-510.

15. Sauter E, Buckwalter JA, McKinley TO, Martin JA. 2012. Cytoskeletal dissolution blocks oxidant release and cell death in injured cartilage. J Orthop Res 30: 593-598.

16. Chen CT, Bhargava M, Lin PM, Torzilli PA. 2003. Time, stress, and location dependent chondrocyte death and collagen damage in cyclically loaded articular cartilage. J Orthop Res 21: 888-898.

17. Buckley MR, Gleghorn JP, Bonassar LJ, Cohen I. 2008. Mapping the depth dependence of shear properties in articular cartilage. J Biomech 41: 2430-2437.

18. Ugryumova N, Jacobs J, Bonesi M, Matcher SJ. 2009. Novel optical imaging technique to determine the 3-D orientation of collagen fibers in cartilage: Variable-incidence angle polarization-sensitive optical coherence tomography. Osteoarthr Cartilage 17: 33-42.

19. Milentijevic D, Rubel IF, Liew ASL, Helfet DL, Torzilli PA. 2005. An in vivo rabbit model for cartilage trauma: A preliminary study of the influence of impact stress magnitude on chondrocyte death and matrix damage. J Orthop Trauma 19: 466.

20. Bulkley GB, Zuidema GD, Hamilton SR, et al. 1981. Intraoperative determination of small intestinal viability following ischemic injury: A prospective, controlled trial of two adjuvant methods (doppler and fluorescein) compared with standard clinical judgment. Ann Surg 193: 628.

21. Carter MS, Fantinl GA, Sammartano RJ, et al. 1984. Qualitative and quantitative fluorescein fluorescence in determining intestinal viability. Am J Surg 147: 117-123.

22. Williams RM, Zipfel WR, Tinsley ML, Farnum CE. 2007. Solute transport in growth plate cartilage: In vitro and in vivo. Biophys J 93: 1039-1050.

23. Ugryumova N, Attenburrow DP, Winlove CP, Matcher SJ. 2005. The collagen structure of equine articular cartilage, characterized using polarization-sensitive optical coherence tomography. J Phys D 38: 2612.

24. Lewis JL, Deloria LB, Oyen-Tiesma M, et al. 2003. Cell death after cartilage impact occurs around matrix cracks. J Orthop Res 21: 881-887.

25. Brockbank KGM, MacLellan WR, Xie J, et al. 2008. Quantitative second

harmonic generation imaging of cartilage damage. Cell Tissue Banking 9: 299-307.

26. Changoor A, Coutu JP, Garon M, et al. 2011. Streaming potential-based arthroscopic device is sensitive to cartilage changes immediately post-impact in an equine cartilage injury model. J Biomech Eng 133: 278.

27. Wilson W, van Burken C, van Donkelaar C, et al. 2006. Causes of mechanically induced collagen damage in articular cartilage. J Orthop Res 24: 220-228.

28. Pan Y, Li Z, Xie T, Chu CR. 2003. Hand-held arthroscopic optical coherence tomography for in vivo high-resolution imaging of articular cartilage. J Biomed Opt 8: 648-654.

29. Li X, Martin S, Pitris C, et al. 2005. High-resolution optical coherence tomographic imaging of osteoarthritic cartilage during open knee surgery. Arthritis research & therapy 7: R318.

30. Sun Y, Responte D, Xie H, et al. 2012. Nondestructive evaluation of tissue engineered articular cartilage using time-resolved fluorescence spectroscopy and ultrasound backscatter microscopy. Tissue Engineering Part C: Methods 18: 215-226.

31. Chu CR, Lin D, Geisler JL, et al. 2004. Arthroscopic microscopy of articular cartilage using optical coherence tomography. Am J Sports Med 32: 699-709.

32. Kaleva E, Virén T, Saarakkala S, et al. 2011. Arthroscopic ultrasound assessment of articular cartilage in the human knee joint A potential diagnostic method. Cartilage 2: 246-253.

33. Witte T, Knill K, Wilson A. 2004. Determination of peak vertical ground reaction force from duty factor in the horse (equus caballus). J Exp Biol 207: 3639-3648.

34. Kurz B, Jin M, Patwari P, et al. 2001. Biosynthetic response and mechanical properties of articular cartilage after injurious compression. J Orthop Res 19: 1140-1146.

35. Ewers B, Dvoracek-Driksna D, Orth M, Haut R. 2001. The extent of matrix damage and chondrocyte death in mechanically traumatized articular cartilage explants depends on rate of loading. Journal of Orthopaedic Research 19: 779-784.

36. Loening AM, James IE, Levenston ME, et al. 2000. Injurious mechanical compression of bovine articular cartilage induces chondrocyte apoptosis. Arch Biochem Biophys 381: 205-212.

37. Saxena R, Sahay K, Guha S. 1991. Shear properties of articular cartilage of a bovine knee joint subjected to moderate and high loads: An experimental study. Proc Inst Mech Eng Part H J Eng Med 205: 89-93.

38. Atkinson T, Haut R, Altiero N. 1998. Impact-induced fissuring of articular cartilage: An investigation of failure criteria. J Biomech Eng 120: 181-187.

39. Buckwalter JA, Brown TD. 2004. Joint injury, repair, and remodeling: Roles in post-traumatic osteoarthritis. Clin Orthop 423: 7.

40. Martin J, Buckwalter J. 2006. Post-traumatic osteoarthritis: The role of stress induced chondrocyte damage. Biorheology 43: 517-521.

CHAPTER 3

VARIABLE RESPONSES OF CARTILAGE TO IMPACT BETWEEN JOINTS AND IMPLICATIONS FOR THE DEVELOPMENT OF POST TRAUMATIC OSTEOARTHRITIS

[1]Kira D. Novakofski, [2]Lise C. Berg, [3]Ilaria Bronzini, [1]Lisa A. Fortier

[1]Department of Clinical Sciences, Cornell University, Ithaca, New York; [2]Department of Clinical Veterinary and Animal Science, University of Copenhagen, København, Denmark; [3]Department of Comparative Biomedicine and Food Science, University of Padova, Padova, Italy

ABSTRACT

Osteoarthritis (OA) affects multiple joints. Studies typically evaluate a single joint or subset of joints, and the results are extrapolated to other, unrelated joints. In the present study, adult equine cartilage explants were harvested from eight major joints including the shoulder (SH), elbow (EL), carpal (CA), metacarpophalangeal (MC), patellofemoral (FP), tarsal (TA), metatarsophalangeal (MT), and proximal interphalangeal (PP) joints, and were injured by compressing with 30 MPa within 1 second. Cell density, cell death, and gene expression were quantified. There were no statistical differences in cell density as a function of depth between joints. Overall injured samples had significantly higher cell death (17.55%, SE=0.01) than non-injured samples (4.62%, SE=0.01, $p<0.0001$). Injury and joint had significant effects on cell death ($p<0.0001$). Expression of *COL2A1* in controls was 13.9x lower in FP ($p=0.0114$) and 9.6x lower in SH ($p=0.0460$) than PP. Expression of *CD-RAP* in controls was 16.3x higher in PP ($p=0.0098$) and 14.6x higher in TA ($p=0.0202$) than FP. After injury, the change in *CD-RAP* expression increased 204% in FP over MC ($p=0.0460$). These results suggest that different joints have varying baseline characteristics and response to injury and may have different susceptibility to developing post-traumatic OA.

INTRODUCTION

Osteoarthritis (OA) is a disease that affects the worldwide population.[1] OA research is most often focused on a single joint, and these findings are then expanded to other unrelated joints. Presently, OA treatments and procedures are based on the concept that articular cartilage throughout the body is similar and that same treatment should be effective for all joints. With this inference, there is an assumption that joints are similarly susceptible to OA. Yet, the incidence of OA is not the same between different joints. In 500 patients with OA, the distribution of 847 affected joints was 41.2% in knees, 30.0% in hands, 19.0% in hips, 4.4% in the tarsus, 3.2% in shoulders, 1.6% in elbows, and 0.6% in the carpus.[2] The hand can be subcategorized to further demonstrate this variability, where the prevalence of OA in the proximal interphalangeal and metacarpophalangeal joints in 1300 women was 16.5% and 6.8%, respectively.[3] Within a single joint with compartmentalized articulating surfaces, such as the knee, there is varying incidence of OA. In a three year study, 24% of patients had radiographic signs of OA in the patellofemoral joint alone, 4% in the tibiofemoral joint, and 41% in both regions of the knee.[4] Despite these differences in incidence of OA, the characteristics of multiple, OA-susceptible joints have not been widely compared to each other. Understanding the differences of healthy cartilage and the resilience to injury between different joints can help facilitate the development of OA therapeutics.

Susceptibility to OA may be due to differences in stimuli response or biochemical or biomechanical properties in cartilage between joints. These differences have been shown in a small subset of joints. Knee and ankle cartilage respond differently to stimuli. Cytokine stimulation with interleukin-1β decreases the synthesis of glycosaminoglycans (GAGs) in the knee more than in the ankle.[5] Mechanical stimulation increases aggrecan expression in the knee but does not change aggrecan

expression in the ankle.[6] Knee and ankle cartilages have different biochemical and mechanical properties. GAG content and dynamic stiffness are higher in the talocrural joint than tibiofemoral or patellofemoral joints.[7] If differences exist in this small subset of joints, differences might occur more widely among joints than previously thought.

Cartilage properties are also highly variable within a single joint. The mean and maximal cartilage thickness of the same site within a single joint cavity varies between patients.[8] In the knees of 27 patients, the thickest cartilage was determined to be on the patella in 22 patients, lateral tibia in three patients, and femoral trochlea in two patients.[9] In the patella, maximal thickness from six normal cadaveric human knees varied 3.8-5.3 mm.[10] In the tarsocrural joint, maximal thickness of the inferior tibial cartilage in 16 people varied 1.08-2.29 mm, as measured by MRI.[11] If the same injurious load were applied to each of these individual cartilages, a different peak stress and strain would likely occur. Within the knee and ankle, mechanical properties of cartilage differ between regions of close proximity.[12,13] The same traumatic stress would likely result in different damage depending on the specific site of injury.

These biochemical and mechanical properties may result from differences in cell activity or density, or corresponding cartilage thickness. Chondrocyte density inversely correlates with the thickness of cartilage: thinner cartilage has a higher cell density (as many as 330,000 mm^{-3}), while thicker cartilage has a lower cell density (up to 14,000 mm^{-3}).[14] In addition, the cell density in the superficial layer of thick cartilage has a lower cell density than thin cartilage.[14] While the thickness of cartilage has been shown to be unrelated to the normal standing stress,[15] lower weight-bearing regions have higher cell-to-matrix ratio than higher weight-bearing regions.[16] The density of cells and how stress is distributed throughout the articulating surface may both be a factor in resiliency to cartilage damage and development of OA.

Current literature suggests that variability between major joints exists, both with respect to baseline cellular density, synthesis activities, and in response to injury. While injury has been well established to cause cell death in cartilage,[17,18] difference between multiple joints in response to injury has not been studied. Understanding these differences will lead to be a better understanding of the unique progression of post-traumatic OA (PTOA) between joints and creation of more joint specific OA treatments. The goal of the present study was to evaluate cartilage in eight major joints, with the hypothesis being that cartilage in different joints would be inherently different, and joints with decreased *in vitro* cell death and increased post-injury anabolic gene expression would be the same joints that have a lower incidence of OA.

METHODS

Tissue collection and injury model

Six millimeter diameter biopsy punches of full thickness cartilage were harvested aseptically from young adult horses (ages 2.5-4 years, n=4) immediately after euthanasia with approval from the Institutional Animal Care and Use Committee. Articular cartilage was harvested from the high impact region of *caput humeri* of the shoulder joint (SH), *condylus lateralis radii* of the elbow joint (EL), proximal surface of *os carpale III* of the carpal joint (CA),[19] *condylus lateralis metacarpi III* of the metacarpophalangeal joint (MC),[20,21] *condylus lateralis phalanx proximalis III* of the proximal interphalangeal joint (PP), *condylus lateralis femoris/trochlea ossis femoris* of the patellofemoral joint (FP),[22] the distal surface of *os tarsi centrale* of the tarsal joint (TA),[22] *condylus lateralis metatarsi III* of the metatarsophalangeal joint (MT).[20-22] Cartilage was grossly evaluated and scored using the International Cartilage Repair Society Clinical Cartilage Injury Evaluation System - 2000.[23,24] Explants were equally divided into control and injury groups and then equally distributed for either imaging

or gene expression analysis (Fig. 3.1). Cartilage explants that were used for imaging were marked with standard permanent-marker ink at harvest to ensure that all images were acquired in the same anterior-posterior orientation. Explants were placed in phenol red-free MEM with 25 mM Hepes, 100 IU/ml penicillin, and 100 μg/ml streptomycin.

Explants were briefly removed from media and placed in a custom-chamber containing the described media. The chamber was then placed under 2.25 mm-diameter indenter on an EnduraTEC ELF3200 mechanical test frame (EnduraTec, Minnetonka, MN). The articular surface was injured with a single compression of 30 MPa[25] within 1 second. After injury, explants for imaging were immediately replaced into media and incubated for 60 minutes at 37°C at 5% CO_2 to allow any immediate biological changes and cell death to occur. Gene expression explants were transferred to Ham's F-12 medium, containing 25 mM Hepes, 2 mM L-glutamine, 50 μg/ml ascorbic acid, 30 μg/ml α-ketoglutaric acid, and 10% FBS and incubated for 48 hours at 37°C at 5% CO_2 to capture changes in expression of a diverse profile of genes.

Multiphoton data acquisition and analysis

After the 60 minute incubation, explants were cut in cross-section and placed in 1 μM sodium fluorescein (AK-FLUOR 25%, Akorn, Inc., Lake Forest, IL) in PBS for multiphoton microscopy (MPM) imaging. Images were collected using a Tsunami titanium:sapphire laser (Newport Corp., Irvine, CA) with 780 nm wavelength at 100 fs pulses and 80 MHz. Emission spectra were collected through a 670 nm long-pass dichroic and photomultiplier tubes using filters of 380-490 nm to collect second harmonic generation, and 510-650 nm to collect fluorescein emission.

To quantify cell density, images from normal controls were converted to binary images using Fiji with Sauvola local threshold.[26] Binary images were then

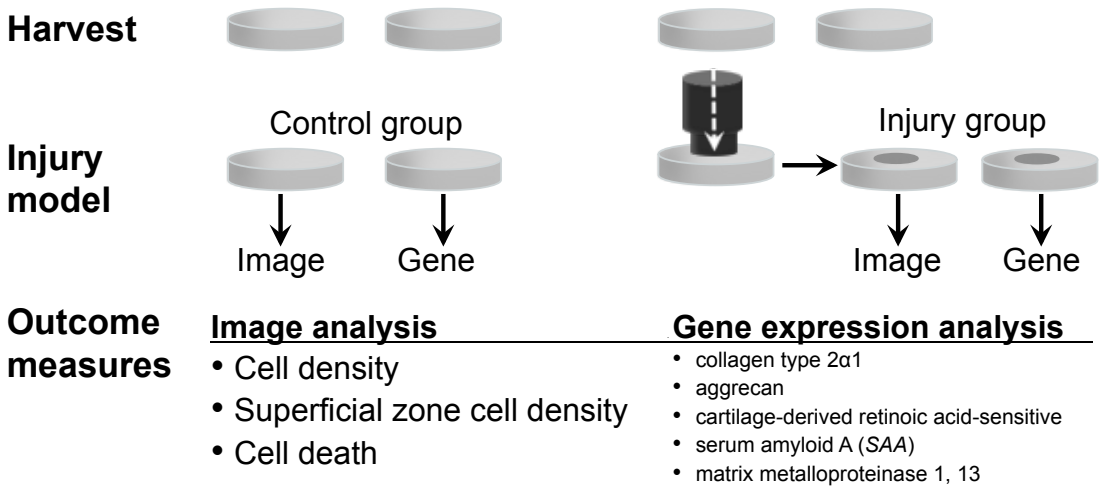

Figure 3.1. Schematic of methods. Biopsy punches (diameter=6 mm) were harvested (n=4 animals), divided equally into control and injured groups, and distributed to image or gene expression analysis.

processed with custom code in MATLAB (MathWorks, Natick, MA) to identify and quantify all chondrocyte profiles as a function of depth, using 50 μm binning. The relationship of cell density and depth for each sample was evaluated by fitting an exponential decay curve to the data points to characterize how the density of cells changed from the articular surface to the deep zone. The exponential decay curve's decay rate length ("b", where b=x in $y=Ae^{-x/b}$) was quantified for each individual sample to give a numerical characteristic to describe the change in cell density with depth. A smaller value of decay rate length indicates a relatively dense region of cells at the surface and a significantly less dense region of cells in the middle and deep zones. A larger value of decay rate length indicates a more uniform distribution of cells among the surface, middle, and deep zones. This decay rate length was compared between joints.

To quantify superficial zone cell density, cells from the superficial zone were identified in the above described images by selecting those cellular profiles that demonstrated an orientation within [-16°, 16°]. A histogram distribution of cellular profiles with 50 μm binning was calculated to determine the maximum density and depth at which maximal density occurred. Cell death was manually quantified in normal controls and injured samples using 50 μm binning.

Gene expression analysis

After 48 hours, explants for gene expression were rinsed in PBS, transferred to RLT lysis buffer (Qiagen, Germantown, MD), snap frozen in liquid nitrogen, and stored at -80°C until processing. The explant and buffer were pulverized in liquid nitrogen using mortar and pestle. Then total RNA was isolated using the RNeasy Fibrous Tissues mini kit (Qiagen). Species-specific intron-spanning equine primers were used to

amplify cartilage genes collagen type 2α1 (*COL2A1*), aggrecan (*AGG*), cartilage-derived retinoic acid-sensitive protein (*CD-RAP*), and inflammatory genes serum amyloid A (*SAA*), matrix metalloproteinase 1 (*MMP-1*), and *MMP-13*. Primers are listed in Table 3.1. Quantitative real-time RT-PCR (qPCR) was performed using the LightCycler® Fast Start DNA Master SYBR Green I and LightCycler ® Real-Time PCR System (Roche Diagnostics, Indianapolis, IN). Results were calculated using the efficiency corrected calculation method also known as the Roche Applied Sciences E(efficiency)-method: Normalized relative ratio = $E_t^{\text{CT (target calibrator)} - \text{CT (target sample)}} / E_r^{\text{CT (reference calibrator)} - \text{CT (reference sample)}}$.[27] Results were normalized to 18S. Expression in control samples are reported as normalized Cp, with higher normalized Cp values indicating higher gene expression.

Statistical analysis

Differences in cell density exponential decay, maximal cell density within the superficial zone, and depth of maximal density within the superficial zone were evaluated using an ANOVA, using SPSS version 21 (IBM Corporation, Armonk, NY). Significance of association between injury and percentage death of cells was evaluated using a t-test. Significance of association between the joint and death was evaluated using an ANOVA. Factors that were found to be significant were then evaluated together in a multivariate regression analysis to determine the effect of each factor while controlling for the effect of the other factors. The potential confounding effect of the depth was controlled for in the multivariate analysis by including it as a co-variate. Because data were clustered by animal, the potential random effect of horse was evaluated by adding the animal as a random effect factor in the analysis.

Gene expression data were analyzed using a Kruskal Wallis non-parametric AOV with Dunn's post-hoc test, using Prism 6 (GraphPad Software, Inc., La Jolla,

Primer name	Primer sequence (5' → 3')	Primer source
18S F 18S R	GAT ACC GCA GCT AGG AAT ATC TGT CAA TCC TGT CCG	DQ222453.1
Aggrecan F Aggrecan R	CTT AGA GGA CAG AAA GCG AC ACT TTG GGC GGA AGA AGG	Trumble *et al* [31]
CD-RAP F CD-RAP R	ATG CCC AAG CTG GCT GA CTT CGA TTT TGC CAG GTT TC	EF679787
Collagen type 2α1 F Collagen type 2α1 R	TCT GCA GAA TGG GCA GAG GTA TA GAT AAT GTC ATC GCA GAG GAC ATT C	NM_031163
MMP-1 F MMP-1 R	CAG TGC CTT CAG AAA CAC GA GCT TCC CAG TCA CTT TCA GC	AF148882.1
MMP-13 F MMP-13 R	GCT GCC TAT GAG CAT CCT TC ACC TCC AGA CCT GGT TTC CT	NM_00108180 4.1
Serum amyloid A F Serum amyloid A R	CCT GGG CTG CTA AAG TCA TC AGG CCA TGA GGT CTG AAG TG	AF240364.1

Table 3.1. Primers used for real time quantitative RT-PCR. Primers were designed by the authors unless otherwise indicated.

CA). Control normalized gene expression and percent difference between control and injured were evaluated. All significance was evaluated at $p<0.05$.

RESULTS

Chondrocyte density and cell death

The distribution of cells was fit to an exponential decay curve to determine if cell density varied in cartilage between different joints (Fig. 3.2, Table 3.2). The exponential decay rate length of cell density was not statistically different between joints (p=0.289). Maximal decay rate length was found in the FP joint (560 μm, SE=171 μm). Minimal decay rate length was found in the CA joint (234 μm, SE=70 μm). The goodness of fit for the exponential model was evaluated by the correlation R^2. The best fit was found in the MT joint (R^2=0.78, SE=0.06). The least best fit was found in the SH joint (R^2=0.57, SE=0.16).

Density of chondrocyte profiles within the superficial zone was different between joints, varying 0.20-2.54x10^{-3} cells/μm^2 (Fig. 3.3, Table 3.3). The lowest superficial zone cell density was found in the FP, and the highest superficial zone cell density was found in MT in individual samples. MC had the highest mean density and was significantly higher than FP with the lowest density (p=0.001), PP (p=0.001), SH (p=0.003), EL (p=0.002), CA (p=0.005), and TA (p=0.033). MT had the second highest density and was significantly higher than FP (p=0.002), PP (p=0.004), SH (p=0.008), EL (p=0.007), and CA (p=0.016). The depth at which the maximal cell density occurred was not statistically different between joints (p=0.306, Fig. 3.3). Peak density occurred at 0-50 μm in 10% of samples, 50- 100 μm in 60%, 100-150 μm in 27%, and 150-200 μm in 3% of samples. The overall mean depth of peak density was 87 μm (SE=6 μm).

Cell death was compared between control and injury to determine if there was

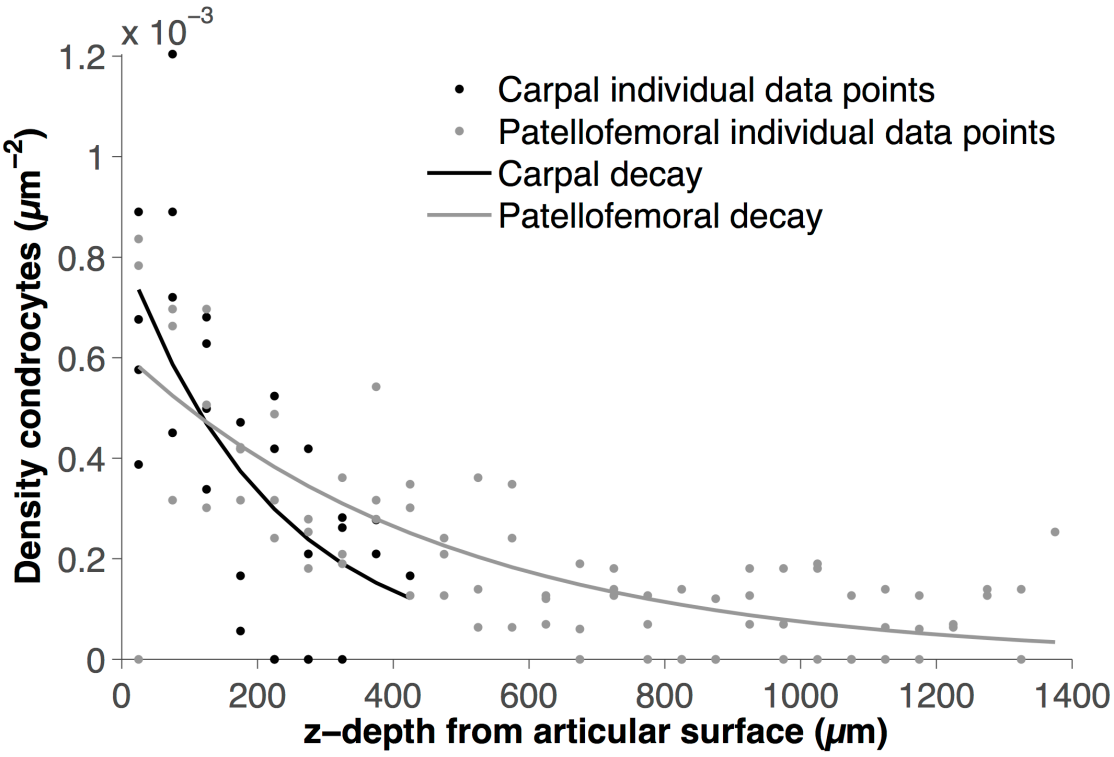

Figure 3.2. Exponential decay rate length of cell density in cartilage. The thickest cartilage with the longest decay rate length was found in the patellofemoral joint (FP, mean=573 μm, SE=190 μm) and is shown with the thinnest cartilage with the shortest decay rate length that was found in the carpal joint (CA, mean=273 μm, SE=71 μm). Lengths of exponential decay rate between joints were not statistically different from each other (p=0.289, n=4).

	SH	EL	CA	MC	PP	FP	TA	MT
Decay length (μm)	573	281	273	345	420	560	236	266
Decay length SE	190	50	71	201	167	170	24	36
R^2	0.56	0.75	0.60	0.71	0.67	0.61	0.77	0.78
R^2 SE	0.17	0.06	0.10	0.16	0.16	0.18	0.16	0.06

Table 3.2. Chondrocyte density decay rate length with goodness of fit as R^2. An exponential decay curve was fit to the data points of cell density as a function of depth. A smaller value has a shorter exponential decay of cell density than a larger value. Cartilage in the shoulder (SH), elbow (EL), carpal (CA), metacarpal (MC), proximal interphalangeal (PP), patellofemoral (FP), tarsal (TA), and metatarsal (MT) joints were evaluated. Decay rate lengths were not statistically different between joints (p=0.289, n=4). SE=standard error.

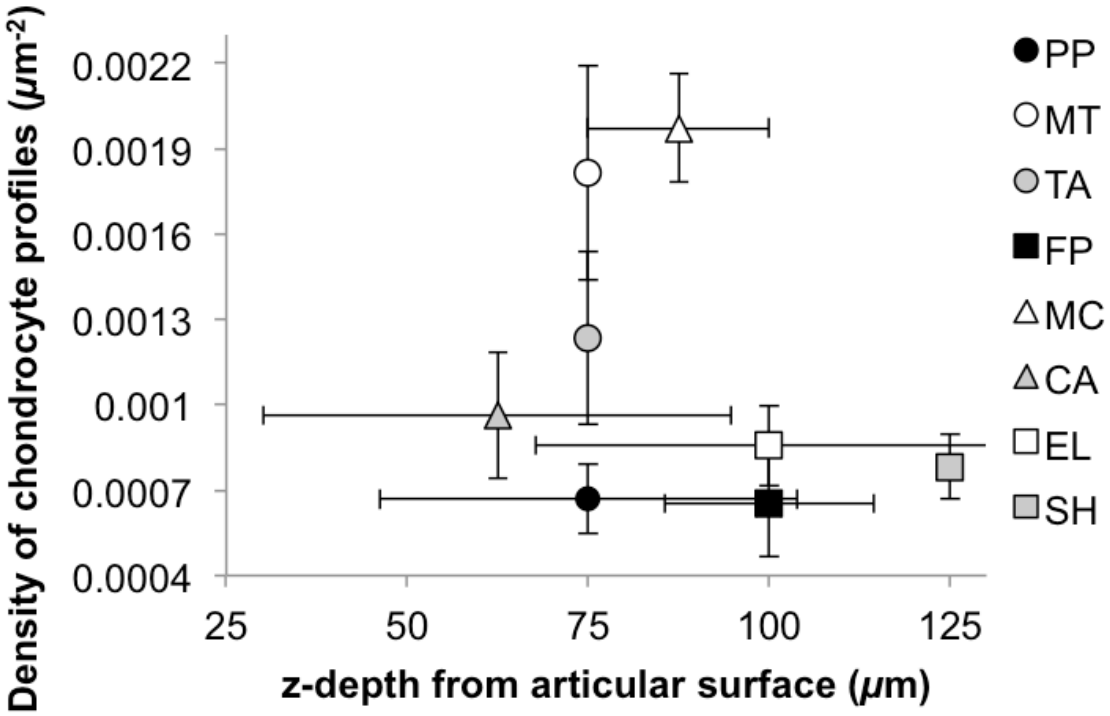

Figure 3.3. Distribution of superficial zone chondrocyte profiles. Peak superficial zone cell density was significantly higher in the metacarpus (MC) than the patellofemoral (FP, p=0.001), proximal interphalangeal (PP, p=0.001), shoulder (SH, p=0.003), elbow (EL, p=0.002), carpal (CA, p=0.005), and tarsal (TA, p=0.033) joints. Density in the metatarsus (MT) was significantly higher than FP (p=0.002), PP (p=0.004), SH (p=0.008), EL (p=0.007), and CA (p=0.016).

	SH	EL	CA	MC	PP	FP	TA	MT
Peak density (10^{-3} cells μm^{-2})	0.78*°	0.86*°	0.96*°	1.97	0.67*°	0.67*°	1.23*	1.8
SE	0.11	0.14	0.22	0.19	0.12	0.12	0.30	0.38

Table 3.3. Distribution of superficial zone chondrocytes. Peak superficial zone cell density was significantly higher in the metacarpus (MC) than the patellofemoral (FP, p=0.001), proximal interphalangeal (PP, p=0.001), shoulder (SH, p=0.003), elbow (EL, p=0.002), carpal (CA, p=0.005), and tarsal (TA, p=0.033) joints. Density in the metatarsus (MT) was significantly higher than FP (p=0.002), PP (p=0.004), SH (p=0.008), EL (p=0.007), and CA (p=0.016). * indicates $p<0.05$ difference from MC; ° indicates $p<0.05$ difference from MT.

a difference in susceptibility to death between joints. Overall injured samples had significantly higher cell death (17.55%, SE=0.01) than non-injured samples (4.62%, SE=0.01, $p<0.0001$). Cell death was significantly different between joints (p=0.010). When analyzing the effect of injury between joints, the regression coefficient of depth from surface was found to be B=0.000, and the random effect of animal was not significant (p=0.704). Depth from surface and animal were therefore not used in the final multivariate regression analysis model. Injury and joint had significant effect on cell death ($p<0.0001$, Table 3.4). Cell death was decreased in controls by B=0.132 ($p<0.001$) with SH used as the reference. Cell death was decreased in SH when compared with MT (p=0.002), TA ($p<0.001$), FP (p=0.032), and EL ($p<0.001$).

Gene expression

Baseline gene expression was evaluated to determine if there were differences in chondrocyte expression between joints (Fig. 3.4). Baseline *COL2A1* expression in controls was 12.4x higher in PP (median Cp=220.85, range 76.92-433.50) than in FP (Cp=17.85, 7.22-25.63, p=0.0114). Basal *COL2A1* was 9.1x higher in PP than SH (Cp=24.35, 21.81-28.46, p=0.0460). Basal *CD-RAP* expression in controls was 23.5x higher in PP (Cp=360.15, 181.10-475.50) than in than FP (Cp=15.32, 12.05-41.80, p=0.0098). Basal *CD-RAP* was 21.7x higher in TA (Cp=331.85, 132.00-441.80) than FP (p=0.0202). No other significant differences in basal gene expression were found (*AGG* p=0.19, *SAA* p=0.05, *MMP-1* p=0.29, *MMP-13* p=0.22).

Changes in gene expression after injury were analyzed to evaluate differences in the gene response of chondrocytes between joints (Fig. 3.4). After injury, the change in *CD-RAP* expression increased 204% in FP (median change=79.10%, range 36.46-393.94%) over MC (change=-55.46%, -71.41 - -45.94, p=0.0460). No significant differences in gene expression between joints were found for the other

Factor	Regression coefficient	SE	p-value
Control	-0.132	0.01	*<0.001*
Injury	0[a]		
PP	0.030	0.014	0.105
MT	0.063	0.020	*0.002*
TA	0.081	0.021	*<0.001*
FP	0.038	0.018	*0.032*
MC	0.031	0.020	0.134
CA	0.024	0.022	0.264
EL	0.079	0.019	*<0.001*
SH	0[a]		

Table 3.4. A multivariate regression analysis was used to determine the of effect from injury ($p<0.0001$) and joint. The effect of the proximal interphalangeal (PP), metatarsal (MT), tarsal (TA), patellofemoral (FP), metacarpal (MC), carpal (CA), and elbow (EL) joints were compared to the effect of the shoulder (SH) joint (i.e., SH was the reference). SE=standard error; [a]parameter set to zero because it is redundant; $p<0.05$ considered significant (italicized).

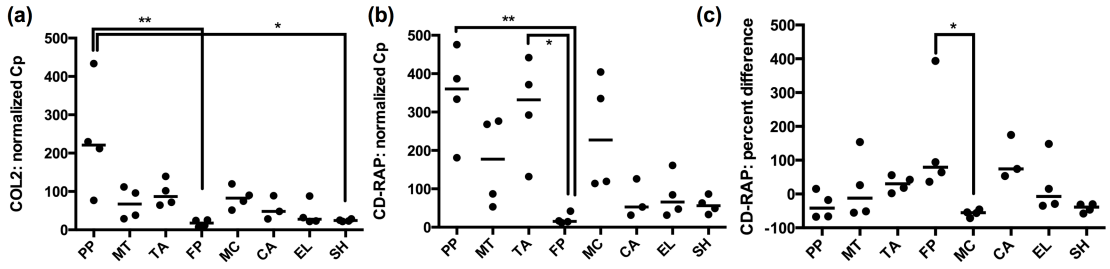

Figure 3.4. (**a**) Baseline collagen type 2α1 (*COL2A1*) was significantly lower in the patellofemoral joint (FP) and shoulder (SH) than proximal interphalangeal joint (PP, **p=0.0114 and *p=0.0460, respectively). (**b**) Cartilage-derived retinoic acid-sensitive protein (CD-RAP) was increased in PP and the tarsus (TA) over FP (**p=0.0098 and *p=0.0202, respectively). (**c**) After injury, CD-RAP was significantly increased in FP over the metacarpus (MC, *p=0.0460). Values above zero indicate increased gene expression, and values below zero indicate decreased gene expression. No statistical differences were found between the metatarsus (MT), carpus (CA), and elbow (EL).

cartilage genes or inflammatory genes (*COL2A1* p=0.05, *AGG* p=0.43, *SAA* p=0.10, *MMP-1* p=0.63, *MMP-13* p=0.22).

DISCUSSION

Comparison of baseline characteristics in normal cartilage and response to injury in eight different joints was performed to better understand the pathogenesis of PTOA. Between joints, differences were found in superficial zone cell density, cell death after injury, and gene expression. These results suggest that joints may have varying susceptibilities to the development of OA.

Cell density was quantified for each joint to determine which joints had differences in exponential decay rate length of cell density from superficial zone to deep zone. The cell density decay rate was not statistically different between joints. This suggests that distribution of cells within cartilage from articular surface to the deep zone was similar between joints, with most cells found in the superficial zone. Similar decay rate lengths between joints, with the peak cell density being found in the superficial zone, is consistent with previous biochemical data comparing FP, TA, and MT, where collagen and GAG concentrations were not significantly different.[22] Similar cellular distribution may result in similar concentrations of collagen and GAG concentrations.

Cell density within the superficial zone was calculated to compare if a zonal difference was present between joints. Cell density in the superficial zone was higher in both the MC and MT than in other joints. Differences previously found in response to stimuli[5,6] and mechanical properties[7,22] may result from the differences in the concentration of superficial zone cells. The peak density of cells in superficial zone was found to be near the similar depth of 87 μm from the articular surface in all joints. If the superficial zone extends to a similar depth in all joints, then the total volume of

middle and deep zones will consequently vary highly between joints. Because cell density decay rate is similar among joints, the volume of low cell density will be different in thin or thick cartilage, with thick cartilage having a larger region of low cell density.

Cell death after trauma was measured to help understand the differences in resiliency to injury between individuals and joints. The random effect of individual animal did not contribute significantly to cell death. While there was individual variability present, one individual was not consistently more resilient to injury than another. The association of different joints with cell death was significant, suggesting unique susceptibility to PTOA between joints. Cell death was increased in TA and FP over SH, and the distribution of OA in major joints is similarly higher in TA and FP than SH.[2] Cell death was also relatively increased in EL over SH; however, EL has less incidence of OA than SH[2] suggesting that cell death is likely only one of multiple factors in OA susceptibility. MT had a higher density of cells in the superficial zone than the other joints, yet had more cell death than SH. Superficial zone density may not be a factor in resilience to traumatic injury, and other factors not examined in the present study such as mechanical properties may contribute to these differences between joints. Images from injured samples were manually counted due to the high irregularity of collagen and fluorescence signals. Decreased emission in the impacted site made identification of cells, dead or alive, difficult and may have lead to a diminished area of damaged tissue being counted, creating a potential lower reported cell death. Yet, significance was found between control and injured despite this potential factor.

Gene expression was quantified to investigate potential differences in cellular activity between joints. Only *CD-RAP* and *COL2A1* expression revealed significant differences. Expression of *CD-RAP* is associated with increased cell proliferation, and

is diminished in severe OA.[28] *CD-RAP* was examined because its expression can change during the very early response to stimuli (<48 hours) and is down-regulated by IL-1β and TGF-β.[30] Synthesis of collagen type II is important for maintaining the cartilage matrix.[29] In the present study, *CD-RAP* and *COL2A1* were expressed less in FP cartilage than in other joints. However, after injury, *CD-RAP* expression was significantly increased in FP compared to MC, yet FP superficial zone density is less than MC. MC and other joints with thin, chondrocyte-dense cartilage may respond differently than thicker joints. This might also suggest that middle and deep zone cells have a different role in gene expression and matrix maintenance than superficial zone cells. An inverse relationship may exist between cartilage zones and gene expression and would need to be further studied for implications in PTOA development.

Overall, differences were found in superficial zone cell densities, cell death, and gene expression between joints. Superficial zone chondrocytes were most dense in MT and MC, implying that cells in this zone may be different between joints. Cell death was relatively increased in MT, TA, FP, and EL over SH. Basal *CD-RAP* and *COL2A1* were lower in FP, yet after injury, *CD-RAP* expression increased significantly more in FP. These differences between joints suggest that findings from a single joint cannot be extrapolated to other joints. The baseline characteristics of chondrocytes in different joints may have an effect on how cartilage responds differently to injury between joints. This may result in different pathologies of PTOA between joints and subsequently in joint-specific future targets for PTOA treatment.

REFERENCES

1. Woolf AD, Pfleger B. 2003. Burden of major musculoskeletal conditions. Bull World Health Organ 81: 646-656.

2. Cushnaghan J, Dieppe P. 1991. Study of 500 patients with limb joint osteoarthritis. I. analysis by age, sex, and distribution of symptomatic joint sites. Ann Rheum Dis

50: 8-13.

3. Haugen IK, Englund M, Aliabadi P, et al. 2011. Prevalence, incidence and progression of hand osteoarthritis in the general population: The framingham osteoarthritis study. Ann Rheum Dis 70: 1581-1586.

4. Duncan R, Peat G, Thomas E, Hay E, Croft P. 2011. Incidence, progression and sequence of development of radiographic knee osteoarthritis in a symptomatic population. Ann Rheum Dis 70: 1944-1948.

5. Eger W, Schumacher BL, Mollenhauer J, Kuettner KE, Cole AA. 2002. Human knee and ankle cartilage explants: Catabolic differences. Journal of orthopaedic research 20: 526-534.

6. Orazizadeh M, Cartlidge C, Wright M, et al. 2006. Mechanical responses and integrin associated protein expression by human ankle chondrocytes. Biorheology 43: 249-258.

7. Treppo S, Koepp H, Quan EC, et al. 2000. Comparison of biomechanical and biochemical properties of cartilage from human knee and ankle pairs. Journal of Orthopaedic Research 18: 739-748.

8. Mühlbauer R, Lukasz S, Faber S, Stammberger T, Eckstein F. 2000. Comparison of knee joint cartilage thickness in triathletes and physically inactive volunteers based on magnetic resonance imaging and three-dimensional analysis. Am J Sports Med 28: 541-546.

9. Eckstein F, Winzheimer M, Hohe J, Englmeier K, Reiser M. 2001. Interindividual variability and correlation among morphological parameters of knee joint cartilage plates: Analysis with three-dimensional MR imaging. Osteoarthritis and Cartilage 9: 101-111.

10. Herberhold C, Faber S, Stammberger T, et al. 1999. In situ measurement of articular cartilage deformation in intact femoropatellar joints under static loading. J Biomech 32: 1287-1295.

11. Al-Ali D, Graichen H, Faber S, et al. 2002. Quantitative cartilage imaging of the human hind foot: Precision and inter-subject variability. Journal of orthopaedic research 20: 249-256.

12. Silverberg JL, Dillavou S, Bonassar L, Cohen I. 2012. Anatomic variation of depth-dependent mechanical properties in neonatal bovine articular cartilage. Journal of Orthopaedic Research .

13. Ugryumova N, Jacobs J, Bonesi M, Matcher SJ. 2009. Novel optical imaging technique to determine the 3-D orientation of collagen fibers in cartilage: Variable-incidence angle polarization-sensitive optical coherence tomography. Osteoarthritis and Cartilage 17: 33-42.

14. Stockwell R. 1971. The interrelationship of cell density and cartilage thickness in mammalian articular cartilage. J Anat 109: 411.

15. Simon WH. 1970. Scale effects in animal joints. I. articular cartilage thickness and compressive stress. Arthritis & Rheumatism 13: 244-255.

16. Eggli PS, Hunzinker EB, Schenk RK. 1988. Quantitation of structural features characterizing weight-and less-weight-bearing regions in articular cartilage: A stereological analysis of medical femoral condyles in young adult rabbits. Anat Rec 222: 217-227.

17. Natoli RM, Scott CC, Athanasiou KA. 2008. Temporal effects of impact on articular cartilage cell death, gene expression, matrix biochemistry, and biomechanics. Ann Biomed Eng 36: 780-792.

18. Sauter E, Buckwalter JA, McKinley TO, Martin JA. 2012. Cytoskeletal dissolution blocks oxidant release and cell death in injured cartilage. Journal of Orthopaedic Research .

19. Palmer JL, Bertone AL, Litsky A. 1994. Contact area and pressure distribution changes of the equine third carpal bone during loading. Equine Vet J 26: 197-202.

20. Brommer H, Brama P, Barneveld A, Weeren Pv. 2004. Differences in the topographical distribution of articular cartilage degeneration between equine metacarpo-and metatarsophalangeal joints. Equine Vet J 36: 506-510.

21. Brama PAJ, Tekoppele JM, Bank RA, et al. 2000. Topographical mapping of biochemical properties of articular cartilage in the equine fetlock joint. Equine Vet J 32: 19-26.

22. Garcia-Seco E, Wilson DA, Cook JL, et al. 2005. Measurement of articular cartilage stiffness of the femoropatellar, tarsocrural, and metatarsophalangeal joints in horses and comparison with biochemical data. Veterinary Surgery 34: 571-578.

23. Brittberg M, Aglietti P, Gambardella R, et al. 2000. ICRS clinical cartilage injury evaluation system-2000.

24. Brittberg M, Winalski CS. 2003. Evaluation of cartilage injuries and repair. The Journal of Bone and Joint Surgery 85: 58.

25. Milentijevic D, Rubel IF, Liew ASL, Helfet DL, Torzilli PA. 2005. An in vivo rabbit model for cartilage trauma: A preliminary study of the influence of impact stress magnitude on chondrocyte death and matrix damage. J Orthop Trauma 19: 466.

26. Sauvola J, Pietikäinen M. 2000. Adaptive document image binarization. Pattern Recognit 33: 225-236.

27. Tellmann G, Geulen O. 2006. LightCycler® 480 real-time PCR system: Innovative solutions for relative quantification. BIOCHEMICA-MANNHEIM- 4: 16.

28. Saito S, Kondo S, Mishima S, et al. 2002. Analysis of cartilage-derivedretinoic-acid-sensitive protein (CD-RAP) in synovial fluid from patients with osteoarthritis

and rheumatoid arthritis. Journal of Bone & Joint Surgery, British Volume 84: 1066-1069.

29. Nelson F, Dahlberg L, Laverty S, et al. 1998. Evidence for altered synthesis of type II collagen in patients with osteoarthritis. J Clin Invest 102: 2115.

30. Kondo S, Cha SH, Xie W, Sandell LJ. 2001. Cytokine regulation of cartilage-derived retinoic acid-sensitive protein (CD-RAP) in primary articular chondrocytes: Suppression by IL-1, bfGF, TGFβ and stimulation by IGF-1. Journal of Orthopaedic Research 19: 712-719.

31. Trumble TN, Trotter GW, Oxford JRT, et al. 2001. Synovial fluid gelatinase concentrations and matrix metalloproteinase and cytokine expression in naturally occurring joint disease in horses. Am J Vet Res 62: 1467-1477.

CHAPTER 4

Hyperoxic treatment after cartilage injury protects against cell death

[1]Kira D. Novakofski, [2]Rebecca M. Williams, [3]Scott A. Rodeo, [1]Lisa A. Fortier

[1]Department of Clinical Sciences, Cornell University, Ithaca, New York; [2]Department of Biomedical Engineering, Cornell University, Ithaca, New York; [3]Department of Sports Medicine, Hospital for Special Surgery, New York, NY, USA

ABSTRACT

Post-traumatic osteoarthritis (PTOA) affects many adults and may not be diagnosed for years after injury. Oxygen has varying roles in supporting and diminishing cartilage function in normal and injured cartilage. In the present study, the effect of intermittent oxygen exposure on chondrocyte viability after injury was evaluated. Bovine cartilage was injured, recovered for 60 minutes, and cultured for 3 days with the following conditions: 5% O_2 — 5% O_2 — 5% O_2 (static normoxic), 5% O_2 — 21% O_2 — 5% O_2 (hyperoxic recovery), 21% O_2 — 5% O_2 — 5% O_2 (hyperoxic injury), and 21% O_2 — 21% O_2 — 21% O_2 (static hyperoxic). Uninjured controls were treated with the same conditions. Cell viability was quantified at the end of the culture duration. Viability in controls was highest in the static normoxic condition (mean=83.6%, SE=3.7%) and lowest in the static hyperoxic condition (mean=73.5%, SE=6.7%). After injury, viability was highest in hyperoxic recovery (mean=60.2%, SE=5.9%) and lowest in static normoxic (mean=51.1%, SE=6.4%). Hyperoxic recovery samples (5—21—5 and 21—21—21) had significantly less cell death after injury (mean= -23.9%, SE=3.8%) than normoxic recovery samples (5—5—5 and 21—5—5, mean= -36.7%, SE=5.3%, p=0.049). This study implies short term, high oxygen exposure has beneficial effects after injury and could have a role in PTOA therapeutic treatment.

INTRODUCTION

Osteoarthritis (OA) is a degenerative disease affecting a large portion of the American and world population.[1-3] OA is a complex disease that has many contributing factors.[1,4] It has been well established that mechanical trauma can result in cell death,[5,6] which leads to post-traumatic OA. There is a growing awareness of the need to investigate PTOA.[7] It is estimated that PTOA contributes to 12% of all OA cases.[3] It is clinically difficult to diagnose PTOA in origin because injury can occur years to decades before clinical symptoms of OA become apparent.[8]

The role of oxygen in cartilage health could have implications in the development of PTOA. Cartilage is avascular and, as a result, has limited oxygen supply. It is estimated that oxygen tension in normal cartilage is about 6% near the articular surface, with decreasing oxygen with depth to as low as 1% oxygen.[9] In OA, oxygen tension is increased in some individuals, with synovial fluid reported to have as high as 9% to 10% O_2.[10,11] Increasing oxygen tension negatively affects cartilage *in vivo*. In adult porcine cartilage, nitric oxide production is lowest when samples are cultured at 1% O_2 compared to 5% or atmospheric 20% O_2.[12] In human OA cartilage, both nitric oxide production and glycosaminoglycan loss from the matrix are increased at 21% O_2 compared to 5% O_2.[13] Oxygen tension also affects the ability of chondrocytes to respond to cytokines. Nitric oxide production is highest in adult porcine cartilage treated with IL-1α and cultured at 20% O_2 compared with 1% O_2.[14] This suggests that higher oxygen tension leads to increased inflammatory mediators which could increase the risk of developing OA. When cartilage is subjected to mechanical loading, the effect of oxygen on the production of inflammatory mediators echoes that which is found with cytokine treatment and oxygen exposure. Nitric oxide production in adult porcine cartilage loaded with 0.05 MPa at 0.5 Hz for 24 hours is lower after culture at 1% O_2 than at 5% or 20% O_2.[12] Overnight pre-treatment of adult

bovine cartilage with super oxide dismutase results in a decreased number of apoptotic cells in four days following injury of 50% strain and 25-29 MPa peak stress.[15] Similarly, N-acetyl cysteine treatment within four hours of injury reduces cell death in mature bovine cartilage.[16] This suggests that increased oxidant scavengers present during injury leads to better long term outcome. This also suggests that higher oxygen tension during injury, or cracking of cartilage leading to higher oxygen exposure in the deeper layers, results in worse outcome after injury and contributes to the development of PTOA.

While many studies report that increased oxygen is detrimental to cartilage, other studies have found it to have beneficial effects. Proteoglycan synthesis in neonatal bovine cartilage is highest at 21% O_2 when compared to oxygen tensions above and below 21%, ranging 3-60% O_2.[17] ATP production is higher when adult porcine cartilage is cultured at 20% O_2 than 1% O_2.[14] Exposure to oxidant treatment can also lead to resilience of chondrocytes to injury. Forty-eight hour pre-treatment with tert-butyl hydrogen peroxide (TBHP), a potent oxidant, resulted in decreased cell death in juvenile porcine cartilage after 5 MPa loading at 1 Hz for 30 minutes compared to non-TBHP-treated controls. Glycosaminoglycan loss from explants to media was also minimized with the use of TBHP pre-treatment. These beneficial effects of TBHP were observed to a certain point—after a maximal concentration of TBHP was reached, increased GAG loss was observed.[18] These studies suggest that oxygen exposure may be beneficial in limited duration and concentration.

The relationship between oxygen and cartilage health is complex. The same work that reported 10% O_2 tension in synovial fluid in naturally-occurring arthritic joints, also reported oxygen tensions as low as 1% O_2.[11] Previous work has shown that chondrocytes grown in alginate at <0.01%, 5%, 10%, or 20% O_2 have decreased total abundance of mRNA at <0.01% O_2. However, cell proliferation was not affected by

hypoxia.[19] It appears that normoxic and hyperoxic conditions both support cartilage health, while hypoxic conditions do not. Although there is not an immediate and direct link between oxygen tension and development or treatment of OA or PTOA, intermittent, strategically applied oxygen exposure could improve cartilage resilience to trauma.

The goal of this study was to evaluate the effect of normoxic (5% O_2) and hyperoxic (21% O_2) conditions during injurious compression, short term recovery after injury, and culture after injury. The hypothesis of this study was that normoxic levels of oxygen during injury, recovery, or culture would lead to increased cell viability and that hyperoxic levels would decrease viability. The results from this study will help to improve the understanding of the pathogenesis of PTOA and help to determine the optimal use of increased or reduced oxygen treatment after traumatic injury.

METHODS

Tissue collection and injury model

Full-thickness cartilage explants (diameter=6 mm) were harvested from bovine, left, distal third and fourth metatarsus. Animals (ages 12-36 months, n=9) were euthanized for reasons unrelated to this study under the guidelines and approval of the Institutional Animal Care and Use Committee. Explants for control or injury were collected from the same condyle (n=4 pairs per animal; n=8 animals). The condyle from each control and injury pair was randomized for subsequent treatment conditions (see Fig. 4.1 for methods schematic). Cartilage was grossly evaluated and scored using the International Cartilage Repair Society Clinical Cartilage Injury Evaluation system - 2000.[20, 21] Only samples receiving a "0" were used for the study.

After explants were harvested, they were immediately submerged into a

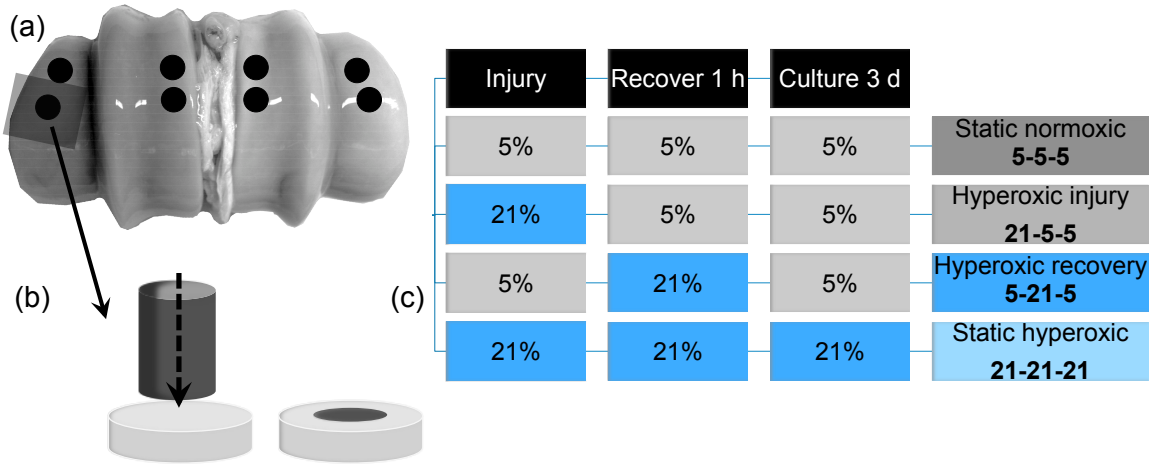

Figure 4.1. Schematic of methods. (**a**) Explants were harvested. Corresponding control and injured explants were collected from the same condyle, with n=4 pairs of explants, as shown in **a**, harvested from each animal (n=8 animals). (**b**) Explants were injured within equilibrated media. (**c**) Each pair of explants was randomized to one of four oxygen conditions.

custom-designed specimen chamber containing media that had been equilibrated overnight to either 5% O_2 or atmospheric (21%) O_2. Media consisted of phenol red-free MEM with 25 mM Hepes, 2 mM L-glutamine, 50 μg/ml ascorbic acid, 30 μg/ml α-ketoglutaric acid, 10% FBS, 100 IU/ml penicillin, and 100 μg/ml streptomycin. Explants and specimen chambers were mounted on an EnduraTEC ELF3200 mechanical test frame (EnduraTec, Minnetonka, MN). Explants were loaded with 30 MPa[22] within 1 second. Explants remained in the same 5% O_2 or atmospheric O_2 equilibrated media, or were transferred to the opposite equilibrated media, and were recovered for 60 minutes at 37°C. After the recovery period, explants were transferred to fresh, pre-equilibrated media of the same 5% O_2 or atmospheric O_2 or were transferred to the opposite equilibrated media, and incubated for 3 days.

The equilibration of O_2 at impact, recovery (1 hour), and culture (3 days) were one of the following four O_2 tension conditions: 5% — 5% — 5% (static normoxic), 5% — 21% — 5% (hyperoxic recovery), 21% — 5% — 5% (hyperoxic injury), and 21% — 21% — 21% (static hyperoxic).

Confocal imaging

After 3 days in culture, explants were removed from the media and cut in half to image the full depth of cartilage in cross section. Explant halves were incubated in 4 μM calcein AM (LIVE/DEAD® Viability/Cytotoxicity Kit for mammalian cells, Invitrogen, Molecular Probes, Eugene, OR) for 15 minutes at 37°C. Then 2 μM ethidium homodimer-1 (LIVE/DEAD® Viability/Cytotoxicity Kit for mammalian cells, Invitrogen) was added, and explants were incubated in calcein AM and ethidium homodimer-1 solution for an additional 15 minutes. Samples were rinsed in PBS and imaged with confocal.

Imaging was performed on a Zeiss LSM510 Meta Axiovert 200 inverted

confocal microscope (Zeiss, Thornwood, NY) with 1.75 μm pixel^{-1} resolution. Calcein AM and ethidium homodimer-1 excitation and emission collection were performed using the recommended wavelengths from the manufacturer. Excitation and emission for each dye were collected in sequential steps, and bleed through into opposing channels was confirmed prior to data acquisition. A tiled 5-step z-scan of x=3.6 mm (axis parallel to articular surface), y=1.8 mm (axis perpendicular to articular surface), and z=50 μm (z-stack of 10 μm intervals) was acquired to encompass normal tissue outside the edge of injury and the full depth of injury from articular surface to deep zone.

Image and viability data analysis

Images from calcein AM and ethidium homodimer-1 were analyzed separately. First, multiple channel, z-stack images were split in Fiji. Resultant images were processed in custom code created in MATLAB R2013a (MathWorks, Natick, MA), which was similar to MATLAB-code "Identifying Round Objects," where chondrocytes were identified as objects. Each calcein AM or ethidium homodimer-1 image was first thresholded to a black and white image (graythresh, im2bw). A smoothing function was applied to objects within an image (bwareaopen), after which any holes in an image were filled (imfill). Objects were further smoothed (imerode) and then dilated (imdilate). Object boundaries were identified (bwboundaries) so that area and perimeter properties could be determined (regionprops). If the area and perimeter were within given threshold values, objects were counted as chondrocytes. Due to the presence of clustered cells, area and perimeter threshold values were used to accommodate single, double, and triple clustered cells. Object counts of chondrocytes were recorded separately for all calcein AM and ethidium homodimer-1 images. Collecting confocal images of a uniform flat plane was not feasible for all samples,

particularly with injured explant samples that had noticeable cracks within the matrix, so cell counts from all z-stack images within one sample were combined and treated as a single viability measure for subsequent statistical analysis.

Statistical analysis

Viability was calculated for each treatment condition. Differences in viability between O_2 tension conditions in uninjured controls were compared using a Kruskal Wallis test in SPSS version 21 (IBM Corporation, Armonk, NY) due to the non-parametric distribution of viability data. To confirm a significant effect of injury on viability, a Mann Whitney test was used to compare the overall mean viability in control to injured explants. Then, the percent difference in viability between control and injured for each corresponding oxygen condition was calculated. To determine the effect of the four oxygen conditions on viability after injury, the percent difference of viability in control and injured explants between oxygen conditions was compared using a Kruskal Wallis test. To evaluate the effect of O_2 tension during recovery on viability after injury, samples recovered at hyperoxia (static hyperoxic and hyperoxic recovery conditions) were grouped together, and samples recovered at normoxia (static normoxic and hyperoxic injury conditions) were grouped together. A Mann Whitney test performed on the percent difference of control and injured viability to compare the two recovery O_2 conditions. A $p<0.05$ was considered significant.

RESULTS

Confocal imaging

Images were acquired with confocal microscopy to demonstrate changes in viability between oxygen conditions and after injury. Live and dead cells were easily identified in both control and injured cartilage explants (Fig. 4.2). In injured samples, the site of

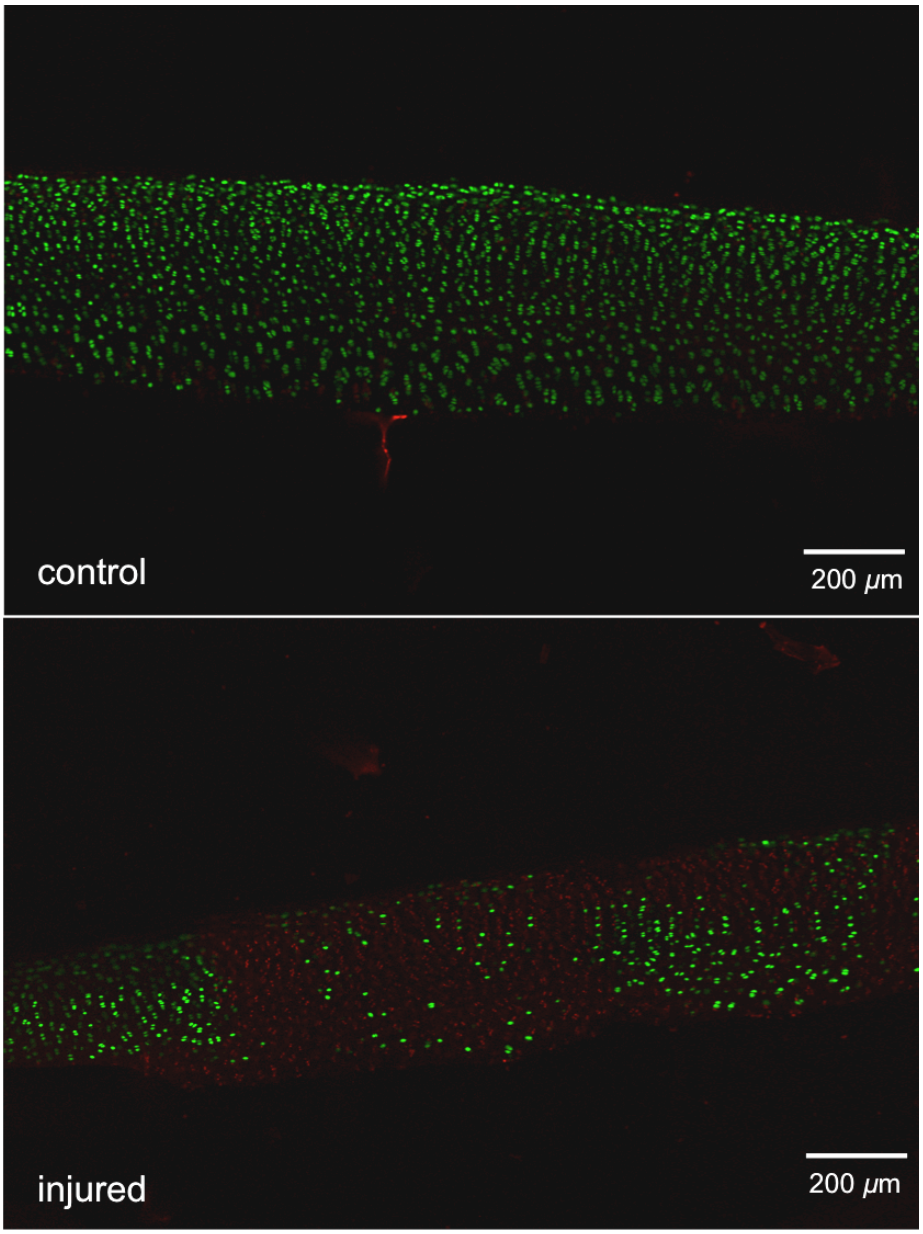

Figure 4.2. Images of control and injured cartilage in the hyperoxic recovery condition group, where the cartilage was injured at 5%, recovered 60 minutes at 21%, and cultured 3 days at 5% O_2. Control cartilage typically had high viability, as indicated by live cell staining with calcein AM (green) and dead cell staining with ethidium homodimer-1 (red). Injured samples had decreased viability.

injury was easily identified in all samples. Most samples had noticeable areas of matrix surface irregularities that could be identified with the unaided eye. When imaging with confocal, cracks were identified that lacked any stained cells, dead or alive, and were noted in most samples.

Effect of oxygen tension on control viability

In uninjured, control samples, cell viability was highest in the static normoxic condition (Fig. 4.3, mean=83.6%, SE=3.7%). With oxygen exposure, viability decreased in uninjured control samples. Viability was decreased by 12.1% in the static hyperoxic condition (mean=73.5%, SE=6.7%) when compared to static normoxic. However, no statistical significance between groups was found ($p=0.311$).

Effect of oxygen tension after injury

The effect of injury on viability was confirmed to be significant prior to performing subsequent statistical analysis between oxygen treatment groups. After injury, viability in all groups was reduced by 31.4% compared to uninjured controls ($p<0.0001$). Differences between oxygen treatment conditions were subsequently evaluated.

The lowest viability after injury was found in the static normoxic condition (Fig. 4.3, mean=51.1%, SE=6.4%), followed by hyperoxic injury condition (mean=52.7%, SE=6.4%). Both static normoxic and hyperoxic injury conditions were recovered at 5% O_2. The highest viability after injury was found to be in the hyperoxic recovery condition (mean=60.3%, SE=5.9%), followed by the static hyperoxic condition (mean=56.8%, SE=4.5%). Both hyperoxic recovery and static hyperoxic conditions were recovered at 21% O_2.

To determine the effect of oxygen conditions after injury, the percent difference between the paired control and injured samples was quantified and

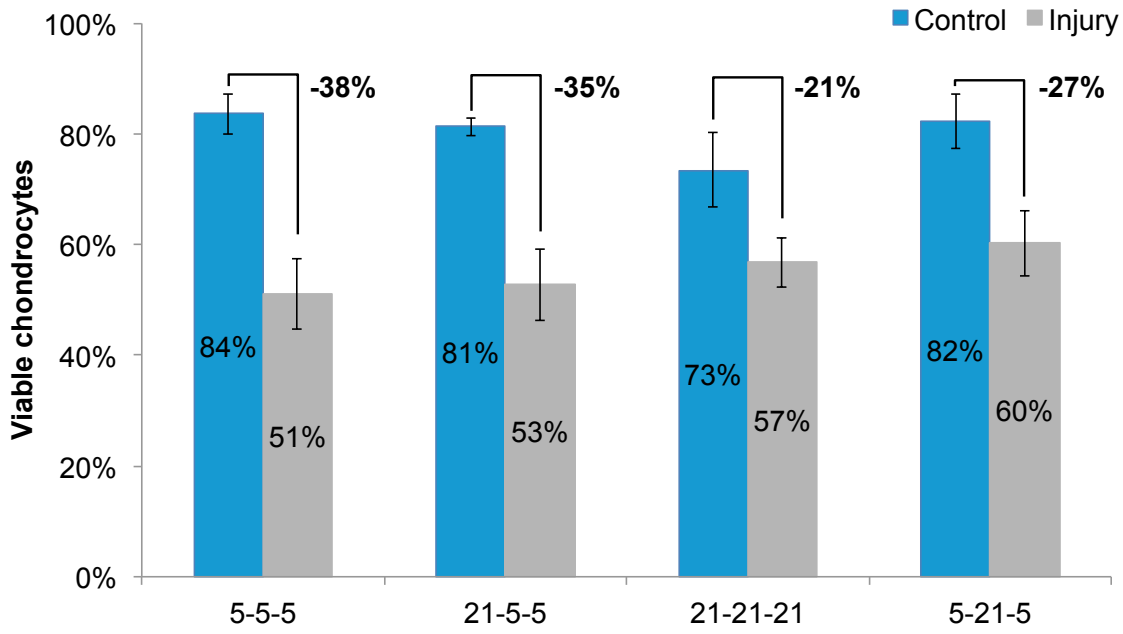

Figure 4.3. Chondrocyte viability with normoxic and hyperoxic treatment. Viability in control samples was highest in static normoxic (5-5-5), where the cartilage was cultured at 5% O_2 for the entire experiment, and lowest in static hyperoxic (21-21-21), where samples were at 21% O_2 for the experiment. After injury, viability was highest in hyperoxic recovery (5-21-5), where samples were injured at 5% O_2, recovered for 60 minutest at 21%, and cultured for 3 days at 21%, and was lowest at the normoxic condition. No significant differences were found between groups.

evaluated. The largest decrease in viability after injury was found in the static normoxic condition (Fig 4.4, mean=-38.2%, SE=7.5%). The next largest decrease was in the hyperoxic injury condition (mean=-35.2%, SE=7.9%). The smallest change in viability after injury was found in the static hyperoxic condition (mean=-20.9%, SE=5.0%), followed by the hyperoxic recovery condition (mean=-26.5%, SE=5.8%). No significant differences were found when comparing the four conditions to each other (p=0.232). To compare the effect of normoxia and hyperoxia recovery, samples recovered at 5% O_2 were clustered together (mean=-36.7%, SE=5.3%) and those recovered at 21% O_2 were clustered together (mean=-23.9%, SE=3.8%). Those that were recovered at normoxia had significantly decreased relative viability after injury compared to those recovered at hyperoxia (p=0.049).

DISCUSSION

This study suggests that oxygen tension affects chondrocyte viability. Hyperoxic treatment of 21% O_2 delivered immediately after injury could reduce long term cell death. This finding implies that hyperoxic treatment has a therapeutic role for injury treatment, including hyperbaric or high oxygen treatments.

The results of this present study found the highest cell viability in uninjured, control samples exposed to 5% O_2. These results support the work of previous studies that have found 5% O_2 to be optimal for maintaining *in vivo* cartilage characteristics during *in vitro* experiments, including matrix permeability, mechanical properties,[23] and glycosaminoglycan concentration.[13] The oxygen tension used in the normoxic condition in the present study most closely represents the oxygen tension found intra-articularly, which is estimated to be 1-6%.[9] Many studies show that cartilage inflammatory mediators[12,14] and apoptosis[15] are decreased with 5% O_2 or decreased oxidant exposure, much work in literature has been and is still consistently performed

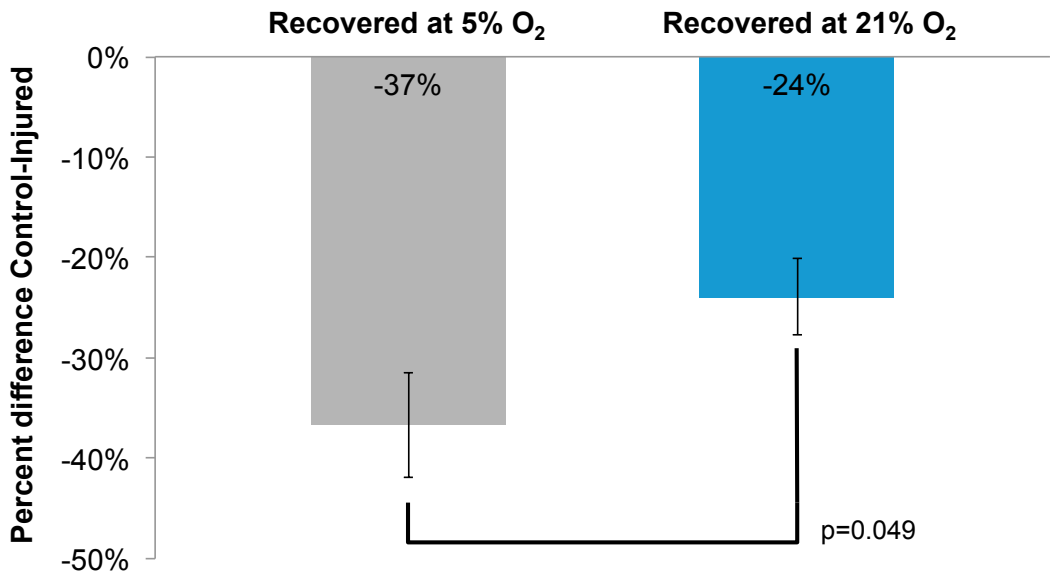

Figure 4.4. Hyperoxic treatment minimized chondrocyte death. The percent difference between control and corresponding injured sample was calculated and compared to determine the overall effect of oxygen on injury. The hyperoxic recovery condition (5-21-5), where samples were injured at 5% O_2, recovered at 21%, and cultured at 5%, had the smallest relative decrease in viability. The static hyperoxic condition (21-21-21), where samples stayed at 21% for the experiment, and the hyperoxic injury condition (21-5-5), where samples were injured at 21% and then recovered and cultured at 5%, had decreasing relative viability, respectively. The static normoxic condition (5-5-5), where samples remained at 5% O_2 throughout the experiment, had the largest relative decrease in viability. Cartilage recovered at hyperoxia (21-21-21, 5-21-5) had significantly less chondrocyte death after injury than those recovered at normoxia (5-5-5, 21-5-5).

at atmospheric 20-21% oxygen. The work in the present study supports these findings—maintaining normal cartilage at atmospheric oxygen results in suboptimal chondrocyte viability. Baseline data collected at 20-21% O_2 is skewed toward increased cell death as shown in the present study, apoptosis,[15] and inflammatory mediators.[12,14]

Chondrocyte viability was highest after injury if immediately treated with hyperoxic 21% O_2 tension. When compared to uninjured controls with the same oxygen treatment, static hyperoxic and hyperoxic recovery conditions had improved viability over static normoxic and hyperoxic injury conditions. This suggests that allowing injured cartilage to recover in hyperoxic conditions reduces cell death associated with trauma. This may result from the increased synthetic activity of cartilage at high oxygen tension.[14,17,19] These benefits were limited to injured cartilage—there was a slight but non-significant decrease in viability found in uninjured cartilage maintained at static hyperoxia. Other studies report limitations to the beneficial effects of hyperoxia. In adult bovine cartilage cultured at 6-91% O_2, samples in oxygen tensions of 24-91% had increased glycosaminoglycan synthesis after 24 hours. However, after this initial time period at high oxygen tension, glycosaminoglycan synthesis decreased. Samples cultured at 6-10% O_2 had relatively steady glycosaminoglycan synthesis.[24] The optimal time of exposure to oxygen still needs to be considered, but the present work combined with previous studies suggests that exposure to high oxygen tension supports cartilage homeostasis.

Translating an *in vitro* hyperoxic environment to a patient-accessible, *in vivo* hyperoxic treatment will be challenging. The most feasible means for increasing oxygen within the joint are by increasing total body oxygen through oxygen inhalation or through increased or modified hemoglobin. Administering high oxygen concentration at hyperbaric pressures can lead to increased oxygen within plasma,

which results in increased synovial fluid oxygen. Hyperbaric oxygen treatment increases oxygen within the joint by over two-fold.[25] Hyperbaric treatment also improves cartilage repair. There is improved healing of full thickness cartilage defects within knees of rabbits given 100% O_2 at 2.5 atm for 2 hours per day for 5 days compared to those not receiving hyperbaric treatment. Improved healing after hyperbaric treatment included decreased chondrocyte apoptosis, increased keratin sulfate synthesis, increased thickness of repair cartilage, and increased number of cells in repair cartilage.[25] Delivering hyperbaric treatment immediately after injury, such as during an athletic event, is not widely available. Hyperbaric treatment requires special equipment, particularly a pressurized chamber. Simple administration of high oxygen at atmospheric pressure will not yield the same increased plasma oxygen or result in the same beneficial healing effects. An alternative approach for increasing oxygen within a joint may be with drug delivery, such as using polymerized hemoglobin to increase total hemoglobin-bound oxygen within the body or an allosteric modifier of hemoglobin to deliver more oxygen to tissue. Extensive testing is needed for general safety and efficacy of these types of drugs for cartilage injury, and there is high risk for abuse with these drugs, particularly with performance enhancement in the athletic field. However, hyperoxic treatment is promising, and optimal oxygen tension and duration of exposure needs to be determined with future work.

REFERENCES

1. Felson DT, Lawrence RC, Dieppe PA, et al. 2000. Osteoarthritis: New insights. part 1: The disease and its risk factors. Ann Intern Med 133: 635.

2. Woolf AD, Pfleger B. 2003. Burden of major musculoskeletal conditions. Bull World Health Organ 81: 646-656.

3. Brown TD, Johnston RC, Saltzman CL, Marsh JL, Buckwalter JA. 2006. Posttraumatic osteoarthritis: A first estimate of incidence, prevalence, and burden of disease. J Orthop Trauma 20: 739-744.

4. Borrelli Jr J, Silva MJ, Zaegel MA, Franz C, Sandell LJ. 2009. Single high-energy impact load causes posttraumatic OA in young rabbits via a decrease in cellular metabolism. J Ortho Res 27: 347-352.

5. Natoli RM, Scott CC, Athanasiou KA. 2008. Temporal effects of impact on articular cartilage cell death, gene expression, matrix biochemistry, and biomechanics. Ann Biomed Eng 36: 780-792.

6. Sauter E, Buckwalter JA, McKinley TO, Martin JA. 2012. Cytoskeletal dissolution blocks oxidant release and cell death in injured cartilage. J Orthop Res 30: 593-598.

7. Anderson DD, Chubinskaya S, Guilak F, et al. 2011. Post-traumatic osteoarthritis: Improved understanding and opportunities for early intervention. J Orthop Res 29: 802-809.

8. Gelber AC, Hochberg MC, Mead LA, et al. 2000. Joint injury in young adults and risk for subsequent knee and hip osteoarthritis. Ann Intern Med 133: 321-328.

9. Zhou S, Cui Z, Urban JPG. 2004. Factors influencing the oxygen concentration gradient from the synovial surface of articular cartilage to the cartilage–bone interface: A modeling study. Arthritis & Rheumatism 50: 3915-3924.

10. Lund-Olesen K. 1970. Oxygen tension in synovial fluids. Arthritis & Rheumatism 13: 769-776.

11. Treuhaft PS, McCarty DJ. 1971. Synovial fluid pH, lactate, oxygen and carbon dioxide partial pressure in various joint diseases. Arthritis & Rheumatism 14: 475-484.

12. Fermor B, Weinberg JB, Pisetsky DS, Guilak F. 2005. The influence of oxygen tension on the induction of nitric oxide and prostaglandin E2 by mechanical stress in articular cartilage. Osteoarthritis and cartilage 13: 935-941.

13. de Isla N, Huselstein C, Mainard D, Stoltz J. 2012. Validation of an in vitro model to study human cartilage responses to compression. Engineering 5: 61-64.

14. Fermor B, Gurumurthy A, Diekman BO. 2010. Hypoxia, RONS and energy metabolism in articular cartilage. Osteoarthritis and Cartilage 18: 1167-1173.

15. Kurz B, Lemke A, Kehn M, et al. 2004. Influence of tissue maturation and antioxidants on the apoptotic response of articular cartilage after injurious compression. Arthritis & Rheumatism 50: 123-130.

16. Martin JA, McCabe D, Walter M, Buckwalter JA, McKinley TO. 2009. N-acetylcysteine inhibits post-impact chondrocyte death in osteochondral explants. The Journal of Bone & Joint Surgery 91: 1890-1897.

17. Clark CC, Tolin BS, Brighton CT. 1991. The effect of oxygen tension on proteoglycan synthesis and aggregation in mammalian growth plate chondrocytes. Journal of orthopaedic research 9: 477-484.

18. Ramakrishnan P, Hecht BA, Pedersen DR, et al. 2010. Oxidant conditioning protects cartilage from mechanically induced damage. Journal of Orthopaedic Research 28: 914-920.

19. Grimshaw M, Mason R. 2000. Bovine articular chondrocyte function< i> in vitro</i> depends upon oxygen tension. Osteoarthritis and Cartilage 8: 386-392.

20. Brittberg M, Aglietti P, Gambardella R, et al. 2000. ICRS clinical cartilage injury evaluation system-2000.

21. Brittberg M, Winalski CS. 2003. Evaluation of cartilage injuries and repair. The Journal of Bone and Joint Surgery 85: 58.

22. Milentijevic D, Rubel IF, Liew ASL, Helfet DL, Torzilli PA. 2005. An in vivo rabbit model for cartilage trauma: A preliminary study of the influence of impact stress magnitude on chondrocyte death and matrix damage. J Orthop Trauma 19: 466.

23. Fermor B, Christensen S, Youn I, et al. 2007. Oxygen, nitric oxide and articular cartilage. Eur Cell Mater 13: 56-65.

24. Ysart GE, Mason RM. 1994. Responses of articular cartilage explant cultures to different oxygen tensions. Biochimica et Biophysica Acta 1221: 15-20.

25. Yuan L, Ueng SW, Lin S, et al. 2004. Attenuation of apoptosis and enhancement of proteoglycan synthesis in rabbit cartilage defects by hyperbaric oxygen treatment are related to the suppression of nitric oxide production. Journal of orthopaedic research 22: 1126-1134.

CHAPTER 5

DISCUSSION, FUTURE DIRECTION, CONCLUSION

Discussion

The research presented in this dissertation was performed to improve the understanding of early cartilage injury using high resolution imaging. The introduction justifies the necessity of high resolution imaging of cartilage and reveals the utility of multiphoton microscopy (MPM) over other *in vivo* imaging techniques. Chapter 2 evaluates the use of MPM for detecting cartilage injury. Chapter 3 characterizes the unique susceptibility of cartilage from different joints to injury. Chapter 4 examines the potential role of increased oxygen tension as an approach to minimize cell death after injury.

Chapter 2 validates the use of high resolution MPM for identifying cartilage injury as a technique that could be adapted for clinical use to further our understanding of post traumatic osteoarthritis (PTOA). Because there is no current *in vivo* method of identifying subtle, early cartilage injury, longitudinal studies of PTOA development are limited. Current studies typically use magnetic resonance imaging (MRI) or computed tomography (CT), both of which have inferior resolution capacities to MPM, to monitor the progression of PTOA after cartilage injury. The presence of a small (<2 μm) crack or a cluster of dead cells in a region of diseased cartilage cannot be monitored with MRI or CT until after significant structural damage (>0.5 mm) has developed. To circumvent this issue in current studies, typically, multiple groups of animals are sacrificed at different time points to collect cartilage so that high resolution imaging of histological sections can be performed. Use of different animals to study disease progression is not an optimal approach for the study of PTOA. Unique patterns of damage between animals that resulted from the same injury were

identified in Chapter 2. This suggests that if using multiple groups of animals to study times points, different damage patterns between animals may affect the findings or lead to high variability. In addition, performing longitudinal studies where *in vivo* microscopy can be performed in place of terminal, histologic imaging would lead to more accurate findings about the progression of PTOA.

Chapters 3 and 4 imply the need for new treatment paradigms. In Chapter 3, MPM was used to characterize the differences in response to injury between joints and suggested that different joints have varying responses to injury with respect to matrix damage and cell death. This is supported by the clinical observation in human and animal patients that different joints have unique susceptibilities to the development of PTOA. This suggests that the application of a universal cartilage treatment after injury is not optimal, and joint specific treatments following injury should be considered. Chapter 4 evaluated the effect of oxygen tension on cartilage injury and unexpectedly found that hyperoxic exposure is protective from chondrocyte death if delivered for short duration immediately after injury. Overall, the work in this dissertation established the application of MPM in *ex vivo* studies for providing a means of collecting quantifiable, high resolution images and the potential for translating this technique to clinical use.

Future direction

Can MPM be adapted for clinical, diagnostic use?

MPM resolves focal cartilage injury and has potential for clinical application. The traumatic loading used in Chapters 2-4 caused cartilage damage that was <0.5 mm in depth, which is below the resolution of MRI and CT. MPM has the potential to be adapted to for arthroscopic application and is being evaluated for clinical use in other fields.[1-4] If a surgeon recommends surgery to a patient based on his/her MRI and/or

CT, during the subsequent arthroscopic procedure, the precise border of a lesion could be located with arthroscopic MPM, "healthy-appearing" regions neighboring degraded regions could be further evaluated, and "healthy-appearing" cartilage in a joint that had other damage, such as a ligament tear, could be further evaluated microscopically. Longitudinal evaluation could be performed, both clinically and in *in vivo* studies. Longitudinal studies would allow further characterization of PTOA progression and development of new treatment algorithms—either drug or rehabilitation in design.

When applied arthroscopically, cartilage damage could be clinically characterized by identifying regions with dead cells (sodium fluorescein), disrupted matrix (second harmonic generation (SHG) and autofluorescence), and optical biomarkers (autofluorescence). The work in Chapter 2 demonstrated the novel use of sodium fluorescein as a dead cell dye. Sodium fluorescein is already FDA approved. Use of this dye would allow the surgeon to identify and quantify region(s) of dead cells, which would subsequently be removed by debridement. This will provide a significantly refined method of cartilage evaluation compared to the current clinical standard of subjective determination of healthy/diseased cartilage based on palpation of the cartilage surface with a metal probe. Sodium fluorescein would also add another tool for diagnostic and research protocols in early PTOA. Longitudinal studies of sodium fluorescein stained regions would determine if cell death truly leads to widespread PTOA and/or if treatments such as hyperoxic, antioxidant, anti-inflammatory, cryotherapy, or rehabilitation immediately after injury could preserve dead cell regions from progressing into diseased tissue and PTOA. Regions with damaged extracellular matrix would be easily identified with SHG and elastin autofluorescence. Longitudinal studies of matrix damage will determine the minimal threshold of damage that leads to PTOA—does a 2 μm crack become larger with time and lead to a widespread area of cartilage matrix with compromised mechanical

integrity? Autofluorescent structures are visible in grossly normal cartilage that neighbors diseased tissue (data not shown). These autofluorescent structures vary in emission wavelength and location (extracellular, intracellular). These structures may serve as optical biomarkers that could be used for future diagnostic application, whether directly with MPM or with adaptation to biochemical assays.

The safety and applicability of MPM for clinical use needs to be further evaluated. MPM utilizes pulsed near infrared (NIR) light during imaging. NIR light is generally considered to be biologically safe. However, the far ends of the NIR range (<800 nm and >1400 nm) have harmful effects. Lower energy, longer wavelength NIR (>1400 nm) causes excitation of water. Imaging with excitation wavelengths >1400 nm can heat the water in tissue and cause thermal damage. Two-photon excitation (TPE) of higher energy, shorter wavelength NIR (<800 nm) can elicit ultraviolet (UV) excitation. Because TPE essentially causes the same excitation as a single photon at half the wavelength, using <800 nm photons with MPM can cause <400 nm excitation and DNA damage. For clinical use, MPM would need to utilize >800 nm to avoid TPE induced UV excitation. NIR excitation >800 nm, however, would not be able to avoid all UV excitation processes because, although low in occurrence, three photon excitation (equivalent to a single photon at a third of the source wavelength) can also elicit UV excitation. Safety testing to examine DNA damage with MPM 800-1400 nm will be needed before clinical application.[5] *Ex vivo* studies, on the other hand, might be better served using <800 nm excitation because second harmonic generation and autofluorescence is stronger at <800 nm wavelengths.

The clinical application of MPM will be challenging due to its field of view and need of relative stability between the imaging surface and MPM objective. The trade-off for providing submicron resolution is a limited field of view (<0.5 mm x <0.5 mm). This is a disadvantage in a clinical setting because the time needed to

evaluate the joint surface would likely exceed 30 minutes. Furthermore, current objective lens designed for *in vivo* use, such as the Olympus Microprobe Objectives, have a working distance of 0.2 mm. This means that the objective needs to be positioned in a parallel plane to and 0.2 mm from the surface of the tissue. This precise positioning could be difficult to obtain during an arthroscopic procedure. Laboratory MPM imaging utilizes low vibration tables. A low vibration adaptation would need to be made for clinical use, such as a locking armature, because the MPM instrumentation could not be hand-held during imaging.

Should future cartilage research continued to be performed in one joint?

The work in Chapter 4 suggests that each joint has different cell distribution and gene expression levels that affect susceptibility to trauma This suggests that findings from studies examining a single joint should not be applied to other joints: studies evaluating chondrocyte death in the distal metatarsus (increased cell death) should not be assumed true for the proximal humerus (decreased death). Multi-joint studies may be more ideal; however, the feasibility of performing these studies is not always possible, particularly in human studies that rely on cartilage collected during joint replacement procedures. Therefore, determining the most representative cartilage for single-joint studies may be a future step. Results in Chapter 4 further suggest thin cartilage may behave differently than thicker cartilage, so single-joint studies may ultimately be limited in the applicability to future clinical work. Overall, different joints might have different pathologies of PTOA, and future work can help to determine the differences in disease progression, which may lead to joint-specific OA treatments.

Could oxygen play a role in future PTOA treatment?

In Chapter 4, hyperoxic treatment was able to minimize cell death after injury. Short duration hyperoxic treatment appears beneficial not only for injured cartilage—previous work has shown that 24 hours at hyperoxic conditions increases glycosaminoglycan synthesis.[6] These *in vitro* findings can be adapted to *in vivo* application. Hyperbaric treatment can increase oxygen concentration in a joint by two-fold and increase keratin sulfate synthesis.[7] Combined, these findings suggest that exposure to high concentrations of oxygen for short time periods of time could help minimize detrimental effects of injury and may have a potential role in mitigating the progression of PTOA. In order for this to be an effective treatment, hyperbaric or hyperoxic treatment would need to be delivered immediately after injury. This short treatment window suggests that a physician appointment within the following day or two is not sufficient. Alternative methods of delivering hyperoxic treatment to joints will need to be developed. Determining the optimal delivery method to patients, oxygen concentration, and duration will need to be evaluated in future work for this potential therapeutic treatment.

Conclusion

The development of PTOA is variable and individualized, both in joints and individual animals and people. Being able to longitudinally evaluate cartilage early with MPM will facilitate the development of early intervening treatments to slow the progression of disease. The etiology of PTOA is diverse, and oxygen may play a role during the very early developments of cartilage damage. While long term exposure to oxygen may exacerbate cell death, it appears the hyperoxic exposure may have a potential application as a therapeutic treatment for cartilage after injury. By understanding the differences between joints and injuries in future studies and being able to identify

subtle injuries in the acute phase with high resolution imaging, the mechanisms of PTOA can be further resolved and new treatments developed.

References

1. Da Costa V, Wei R, Lim R, et al. 2008. Nondestructive imaging of live human keloid and facial tissue using multiphoton microscopy. Archives of Facial Plastic Surgery 10: 38.

2. Pavlova I, Hume KR, Yazinski SA, et al. 2010. Multiphoton microscopy as a diagnostic imaging modality for lung cancer. Proc Soc Photo Opt Instrum Eng 7569: 756918.

3. Wang CC, Li FC, Wu RJ, et al. 2009. Differentiation of normal and cancerous lung tissues by multiphoton imaging. J Biomed Opt 14: 044034.

4. Skala MC, Squirrell JM, Vrotsos KM, et al. 2005. Multiphoton microscopy of endogenous fluorescence differentiates normal, precancerous, and cancerous squamous epithelial tissues. Cancer Res 65: 1180.

5. Cruz JMD, McMullen JD, Williams RM, Zipfel WR. 2010. Feasibility of using multiphoton excited tissue autofluorescence for in vivo human histopathology. Biomedical optics express 1: 1320.

6. Ysart GE, Mason RM. 1994. Responses of articular cartilage explant cultures to different oxygen tensions. Biochimica et Biophysica Acta 1221: 15-20.

7. Yuan L, Ueng SW, Lin S, et al. 2004. Attenuation of apoptosis and enhancement of proteoglycan synthesis in rabbit cartilage defects by hyperbaric oxygen treatment are related to the suppression of nitric oxide production. Journal of orthopaedic research 22: 1126-1134.